Marine and Petroleum Geology 160 (2024) 106611

Contents lists available at ScienceDirect

Marine and Petroleum Geology

journal homepage: www.elsevier.com/locate/marpetgeo

Depositional and sequence stratigraphic controls on diagenesis in the Upper Cambrian-Lower Ordovician Barik Formation, central Oman: Implications for prediction of reservoir porosity in a hybrid-energy delta system

Mohamed A.K. El-Ghali [a,b,*], Olga Shelukhina [c], Iftikhar Ahmed Abbasi [b], Mohamed S.H. Moustafa [b], Osman Salad Hersi [d], Numair A. Siddiqui [e,f], Khalid Al-Ramadan [g], Abdullah Alqubalee [h], Abdulwahab Muhammad Bello [h], Abduljamiu O. Amao [h]

[a] Earth Sciences Research Center Sultan Qaboos University, P.O. Box 34, Postal Code 123, Al-Khoudh, Muscat, Sultanate of Oman
[b] Department of Earth Sciences, College of Science, Sultan Qaboos University, P.O. Box 34, Postal Code 123, Al-Khoudh, Muscat, Sultanate of Oman
[c] Research and Education Center, Novosibirsk State University, Novosibirsk city, Russia
[d] Department of Geology, University of Regina, Regina, Saskatchewan, Canada
[e] Department of Geosciences, Universiti Teknologi PETRONAS, 32610, Bandar Seri Iskandar, Perak, Malaysia
[f] Shale Gas Research Group, Institute of Hydrocarbon Recovery, Universiti Teknologi PETRONAS, 32610, Bandar Seri Iskandar, Perak, Malaysia
[g] Department of Geosciences, College of Petroleum Engineering and Geosciences, King Fahd University of Petroleum and Minerals, Dhahran 31261, Saudi Arabia
[h] Center for Integrative Petroleum Research, College of Petroleum Engineering and Geosciences, King Fahd University of Petroleum and Minerals, Dhahran 31261, Saudi Arabia

ARTICLE INFO

Keywords:
Diagenesis
Reservoir porosity
Hybrid-energy delta
Barik formation
Cambrian-ordovician
Central Oman

ABSTRACT

This study aims to employ an integrated depositional and sequence stratigraphic approach to assess the control of diagenesis on reservoir porosity of a hybrid-energy delta system. The study focuses on examining the outcropped Upper Cambrian-Lower Ordovician Barik Formation representing a highstand system tract of a hybrid-energy delta in the Haushi-Huqf region of Central Oman, which is equivalent to the subsurface gas reservoirs within the Interior Oman Salt Basins. The petrographic, mineralogical, and geochemical assessments revealed that the Barik Formation primarily consists of moderately to very well-sorted coarse-grained siltstones to fine-grained sandstones, with a composition mainly comprisingfeldspathic- and subfeldspathic arenite and the reservoir porosity is controlled by various degrees of diagenetic processes. Eodiagenetic alterations comprise mechanically infiltrated clays and kaolinitization of silicate grains, including detrital feldspars, micas, and mud matrix. The mechanically infiltrated clays (e.g., smectite) were introduced into the sandstones by the percolation of muddy waters under the control of tidal pumps. Although these clays may affect reservoir porosity during eodiagenesis, they positively preserve reservoir porosity during deep burial (mesodiagenesis) by inhibiting cementation by feldspar and quartz overgrowths. Kaolitization of silicate detrital grains was facilitated by the influx of meteoric waters into the sandstones as the delta progrades during the highstand system tract. During progressive burial and lack of extensive eodiagenetic cement, compaction continued and reduced reservoir porosity. Illitization and chloritization of the mechanically infiltrated smectitic clays took place; however, they limited the cementation by quartz and feldspar overgrowths. The quartz and feldspar overgrowths on detrital grains with discontinued smectitic clay coats supported the detrital grains from further compaction and, thus, helped in reservoir porosity preservation. Moreover, extensive feldspar dissolution and kaolinitization has occured during mesodiagenesis and enhanced the reservoir porosity. Subordinate amounts of calcite, dolomite, and gypsum cement have a minor reduction in the reservoir porosity of the Barik Formation. Hence, it can be concluded that, on the one hand, lack of eodiagenetic cementation favored intense reservoir porosity reduction due to compaction. Nevertheless, on the other hand, the mechanically infiltrated clays during the eodiagenetic stage helped preserve the reservoir porosity by hindering the formation of quartz and feldspar overgrowths during the mesodiagenetic stage. This study may serve as an analog model for a similar hybrid-energy delta sandstone reservoirs to better understand

* Corresponding author. Department of Earth Sciences, College of Science, Sultan Qaboos University, P.O. Box 34, Postal Code 123, Al-Khoudh, Muscat, Sultanate of Oman, Earth Sciences Research Center Sultan Qaboos University, P.O. Box 34, Postal Code 123, Al-Khoudh, Muscat, Sultanate of Oman.
E-mail address: melghali@squ.edu.om (M.A.K. El-Ghali).

https://doi.org/10.1016/j.marpetgeo.2023.106611
Received 20 October 2023; Received in revised form 16 November 2023; Accepted 17 November 2023
Available online 23 November 2023

the type, and spatial and temporal of diagenetic alterations and their role in controlling the reservoir quality in deeply buried sandstone reservoirs.

1. Introduction

Sandstones in a deltaic system are essential oil and gas reservoirs globally and spanning from Precambrian to Cenozoic eras (Coleman, 1981; Wright, 1985; Coleman and Roberts, 1989; Bhattacharya and Walker, 1992; Coleman et al., 1998; Dalrymple et al., 2003; Tanabe et al., 2003; Bhattacharya and Giosan, 2003). Sandstones of a deltaic system commonly constitute heterogeneous reservoirs at various scales (i.e., micro-to giga-scale) owing to the vast variability of the depositional and postdepositional (i.e., diagenetic and tectonic) processes (Moraes and Surdam, 1993; Critelli and Nilsen, 1996; Furlan et al., 1996; De Ros, 1998; El-Ghali et al., 2009; Barbera et al., 2011; Caracciolo et al., 2014). However, diagenetic processes exert a substantial control on porosity (i.e., the reservoir storage capacity) and permeability (i.e., reservoir performance) evolution and distribution. Therefore, predicting the reservoir quality evolution and distribution is a key to developing efficient exploration, production, and enhanced recovery strategies as well as subsurface CO_2 and hydrogen storage capacity. Reliable prediction requires a comprehensive knowledge of the diagenetic processes, including cementation, dissolution, replacement, and compaction (Mansurbeg et al., 2008; El-Ghali et al., 2009; El-Ghali et al., 2013; El-Khatri et al., 2015; Siddiqui et al., 2020; Usman et al., 2020; Shelukhina et al., 2021a; Civitelli et al., 2023). Cementation and compaction processes are known for porosity reduction, whereas dissolution as well as fracturing are counted for porosity enhancement. These diagenetic processes are strongly governed by a wide series of interconnected factors, including detrital composition, grain size, sorting, organic matter content, pore-water chemistry, rate of deposition, original porosity and permeability, degree of bioturbation, climatic condition, and burial history (Morad et al., 2000; El-Ghali et al., 2006a-c, 2009; Corrado et al., 2019; Civitelli et al., 2023). Apart from the climatic condition and burial history, knowledge about these controlling parameters can be gained through a well-constrained depositional environment and sequence stratigraphy models (Al Ramadan et al., 2005; El-Ghali et al., 2006a-c; Mansurbeg et al., 2008; El-Ghali et al., 2013). Accordingly, prediction of reservoir quality evolution and distribution can be significantly achieved by linking diagenetic processes within the depositional environment and sequence stratigraphy. Several studies that adopted this research approach have been successfully carried out in fluvial (El-Ghali et al., 2009; El-Khatri et al., 2015; Critelli et al., 2018), shallow marine (Al-Ramadan et al., 2005; El-Ghali et al., 2006c; El-Ghali et al., 2009), deltaic (El-Ghali et al., 2019), deep marine (Mansurbeg et al., 2008; Barbera et al., 2011; Mansurbeg et al., 2013; Amendola et al., 2016; Civitelli et al., 2023; Critelli et al., 2023) and glacial (El-Ghali et al., 2006a-b; El-Ghali et al., 2019) environments. Until now, despite these studies, addressing diagenetic processes for a deltaic environment within sequence stratigraphy is not well constrained (El-Ghali et al., 2013), particularly the fine-grained hybrid energy deltaic environment. The studied fine-grained hybrid energy delta outcrops of Barik Formation in Central Oman are subsurface-equivelant tight-gas reservoirs in the Interior Sedimentary Basins (Buckley, 1997; Al Marjibi, 2011; Shelukhina et al., 2021a, 2021b; Shelukhina, 2021). Consequently, the outcrops of Barik Formation in Central Oman offer an exceptional opportunity to investigate the control of diagenetic processes on porosity evolution and distribution within the depositional environment and sequence stratigraphic contexts. The selection of the Barik Formation outcrops for this study was based on several key factors: (i) the well-exposed nature of the rocks, (ii) the consistent nature of lateral and vertical continuity, (iii) the accessibility for comprehensive logging and sampling, and (iv) the presence of well-documented depositional environment and sequence stratigraphy models supported by previous research (Buckley, 1997; Al Marjibi, 2011; Shelukhina, 2021; Shelukhina et al., 2021b). In this study, the aims are to (i) describe the diagenetic processes, their products, and distribution, (ii) define and understand the depositional environment and sequence stratigraphic parameters that control diagenetic processes, their products, and distribution, and (iii) discuss the control of the diagenetic process, their products, and distribution with the depositional environment and sequence stratigraphy on porosity distribution and evolution. The anticipated outcrop-based diagenetic processes and product model within the depositional environment and sequence stratigraphy and subsequent control on reservoir porosity distribution and evolution can serve as an analog to fine-grained hybrid-energy deltas and subsurface counterparts both regionally and globally.

2. Geological setting of thestudy area

The area of study belongs to Mahatta Humaid area that occupies the northwestern portion of the Haushi-Huqf region of Central Oman (Figs. 1A–B). The Haushi-Huqf outcrops stretch along the southern part of the Arabian Peninsula with a sedimentary record ranging from the Precambrian clastic and carbonae deposits truncated by Cambrian to Cenozoic continental to marine deposits (Fig. 1C; Hughes Clarke, 1988; Buckley, 1997; Forbes et al., 2010).

The studied stratigraphic interval belongs to the Late Cambrian-Early Ordovician Barik Formation outcrops (Fig. 1D; Forbes et al., 2010). During the sag-phase, the deposition took place under a semi-arid to semi-humid climatic condition (Al-Kiyumi, 2019) when Oman was situated in the West Gondwana of about 15° to the south of the equator (Courjault-Rade et al., 1992; Cocks and Torsvik, 2002; Molyneux et al., 2006). Stratigraphically, Barik and the overlying Mabrouk, Barakat, and Ghudun formations along with the underlying Al Bashair Formation, represent the Andam Group (Fig. 1C; Buckley, 1997; Forbes et al., 2010). The Andam Group with the underlying Mahatta Humaid Group and the overlying Safiq Group represent the Haima Supergroup (Fig. 1C; Buckley, 1997; Forbes et al., 2010). In the area of study, the Barik Formation's lower contact is well-exposed; it is a conformable and gradational with the underlying Al Bashair Formation and the upper contact is covered by the Recent sand dunes (Shelukhina, 2021; Shelukhina et al., 2021a, 2021b). In the subsurface Interior Oman Salt Basins, the Barik Formation's lower and upper contacts with Al Bashair and Barakat formations are conformable; respectively (Millson et al., 2008; Forbes et al., 2010; Al Marjibi, 2011). In the area of study, the Barik Formation composite section is about 50 m thick (Figs. 2A–E; Shelukhina, 2021; Shelukhina et al., 2021a, 2021b). The Barik Formation composite section comprises coarse-grained siltstone and very fine-to fine-grained sandstones intercalating with reddish color mudstone that were deposited in a prograding hybrid-energy delta system (Fig. 2A; Shelukhina, 2021; Shelukhina et al., 2021a, 2021b). In the Interior Oman Salt Basins, the subsurface Barik Formation is pinching out northward to marine mudrocks of Al-Bashair Formation (Droste, 1997; Ramseyer et al., 2004). It is reaching a thickness of ca. 800 m and resting between 4000 and 4500 m depth (Ramseyer et al., 2004).

The outcrops of Barik Formation depositional environment and sequence stratigraphy models in the study area (i.e., Mahatta Humaid area) are studied and described by Shelukhina (2021) and Shelukhina et al. (2021b) and depicted in Fig. 2A. The formation consists of four facies associations (i.e., mouth bar/shoreface, tidal flat, tidal channels, and delta distributary channel deposits) representing a fine-grained hybrid-energy delta system (Fig. 2A–E).

The mouth bar/shoreface facies association (Figs. 2A and B)

illustrates the distal portion of the delta. It comprises brown to reddish-brown sheet-like and locally lenticular sandstone bodies. The sandstone bodies are rippled, being predominantly asymmetrical to rarely symmetrical. The asymmetrical ripple bedforms are about 5 cm wide and 1–1.5 cm in height, indicating paleoflow directions to north-northeast and northwest. Flakes and clasts of mudstone are locally present within these sandstones.

The tidal flat facies association (Figs. 2A and C) is predominantly mudstone interbedded with thin fine-grained sandstones and occurs as centimeter- and decimeter-scale thick sheet-like bodies. The sandstones show asymmetrical and symmetrical ripples. The mudstones include both massive and parallel laminated layers. Trace fossils assemblage,

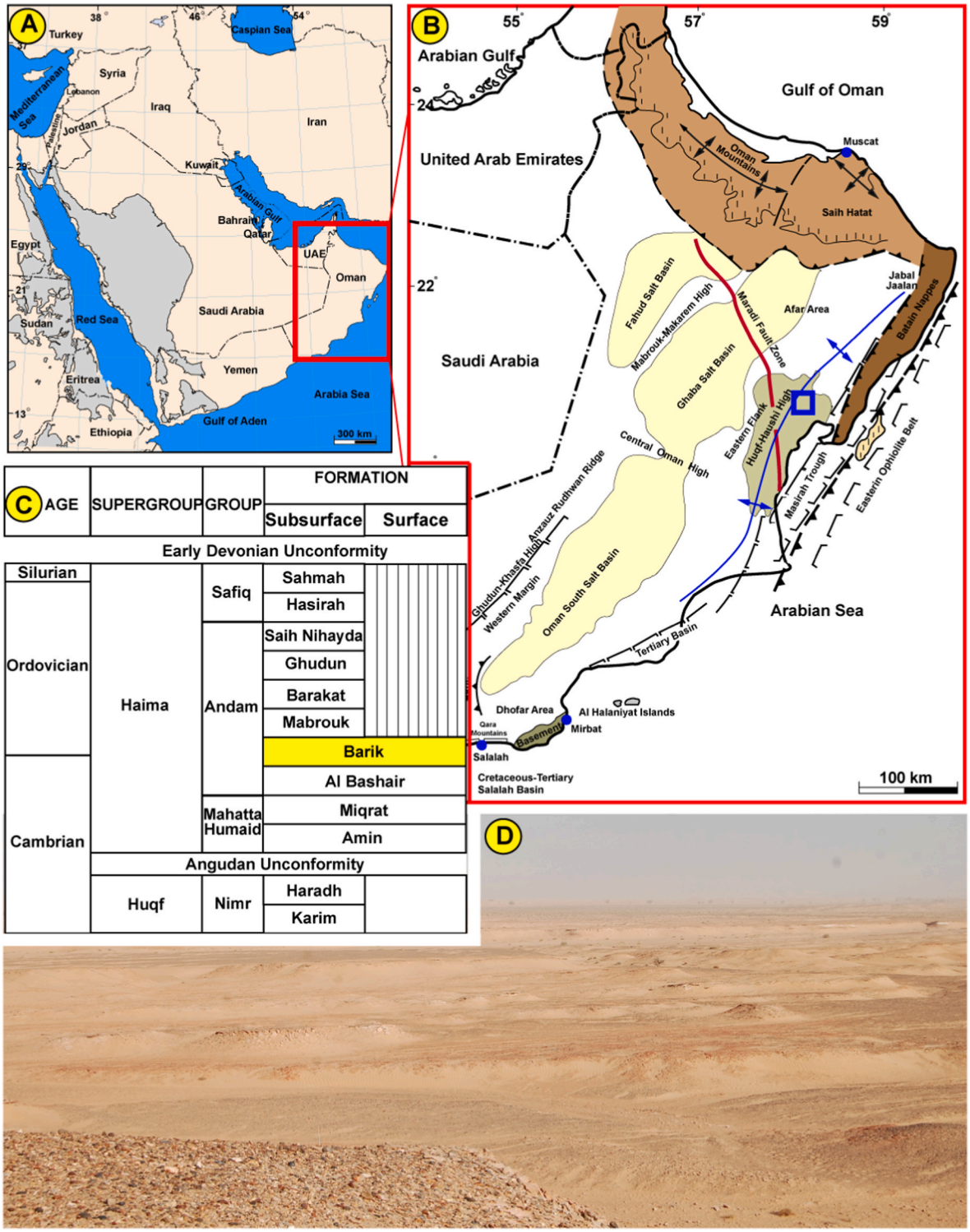

Fig. 1. A sketched location map displaying (A) the position of the Sultanate of Oman on the southeastern portion of the Arabian Peninsula and (B) the position of the area of study, namely Mahatta Humaid of Haushi-Huqf region in Central Oman (modified after Droste, 1997), and (C) a stratigraphic nomenclature of Haima Supergroup showing the position of the studied Barik Formation (After Forbes et al., 2010), and (D) a field photo of the exposed Barik Formation in the Mahatta Humaid of Haushi-Huqf region in Central Oman (After Shelukhina et al., 2021a).

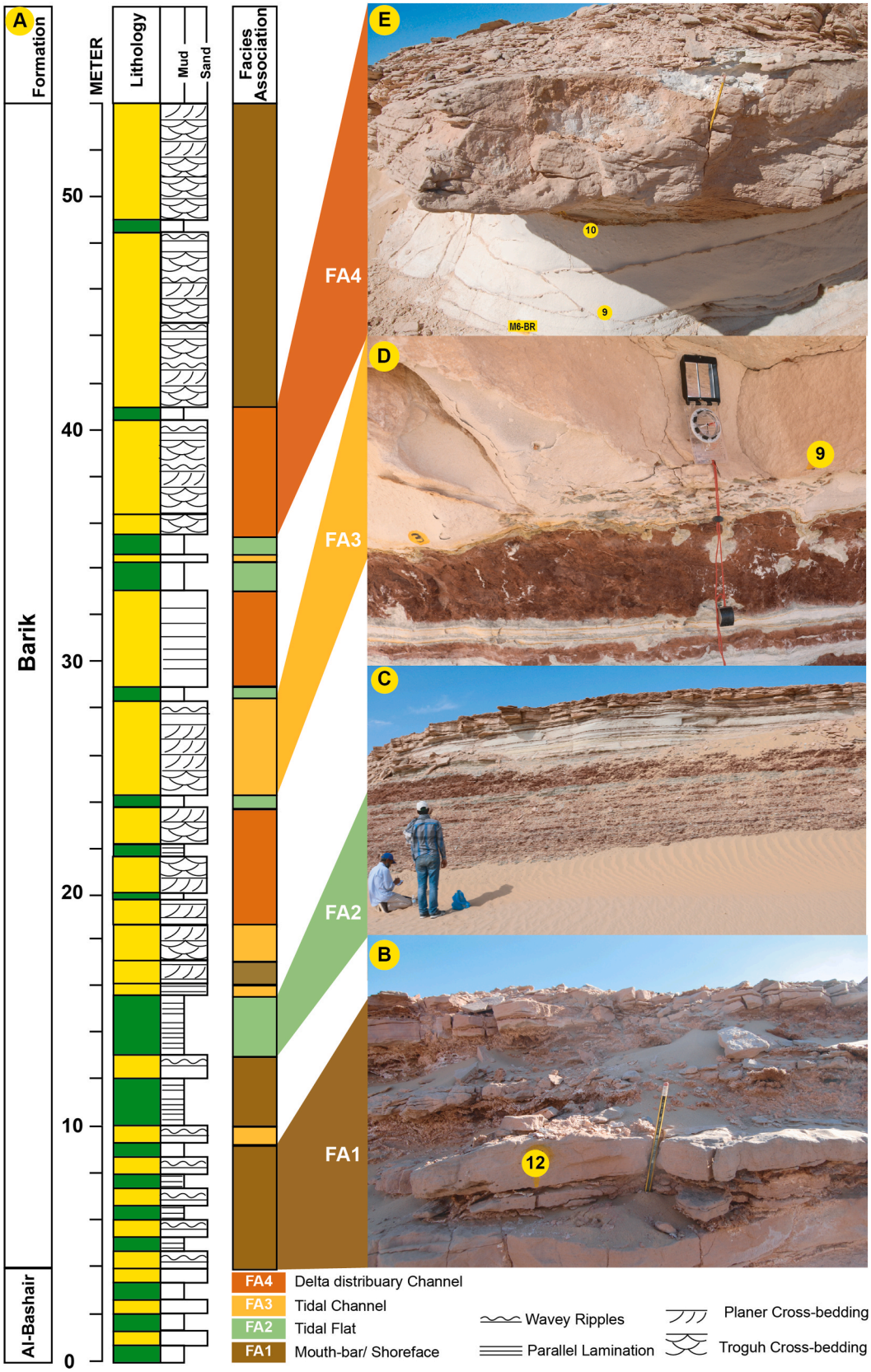

Fig. 2. A detailed sedimentological log with a representative field photos of the Barik Formation outcrops in the Haushi-Huqf region of central Oman depicting (A) lithology, sedimentary structures, and facies associations, (B) mouthbar/shoreface facies association (FA1), (C) tidal flat facies association (FA2), (D) tidal channel facies association (FA3), and (E) delta distribuary channel (FA4).

mainly Skolithos, are typical for this facies association.

The tidal channel facies association (Figs. 2A and D) displays white, sheet-like sandstone and thin mudstone interbeds forming fining upward cycles. In the lower part, this association consists of sandstones with different bedform structures such as horizontal parallel laminated sandstone, low-angle planar and tangential planar cross-bedded sandstone. In contrast, the upper part is comprised of intercalations of climbing asymmetrical rippled sandstone, climbing symmetrical rippled sandstone, and flaser bedded sandstone and mudstone. In addition, trace fossils assemblage, including *Skolithos*, *Planolites*, and *Thalassinoides*, are present in this facies association.

The Delta distributary channel facies association (Figs. 2A and E) encompasses a set of amalgamated channelized sandstone bodies. The lower part shows tangential and sigmoidal planar cross-beds, and trough cross-bedded sandstone. The sandstones are intercalated by thinly laminated, red to green mudstones.

The vertical arrangement, in ascending order, of the recognized facies associations from the deep (i.e., mouth-bar/shoreface) to the shallow (i.e., delta distributary channel) helped in identifying eight parasequences; each parasequence represents a shallowing-upward pattern (Fig. 2A). Thus, the overall vertical arrangements of the identified eight parasequences are characterized by a shallowing- and prograding-upward trend depicting a third-order highstand systems tract (Shelukhina, 2021; Shelukhina et al., 2021b).

3. Materials and methods

This study is based on 152 sandstone samples obtained from 12 described outcropped sections of the Barik Formation in the Haushi-Huqf region of central Oman. The obtained sandstone samples are representative of all the identified facies associations and parasequences of the third-order HST (Figs. 2A–E). The obtained sandstone samples were impregnated with a blue-epoxy resin to recognize and quantify porosity. The impregnated samples were thin sectioned and polished. All polished thin sections were partially stained with Alizarin Red-S to facilitate the recognition and identification of different types of carbonates and with a stain for potassium-feldspar and plagioclase feldspar recognition and identification (Bailey and Stevens, 1960; Dickson, 1966).

Textural analysis was done for all the thin sections to examine the variation and distribution of grain size and sorting. The longest axis of 100 uncompacted and undeformed detrital grains was measured for each thin section. The minimum, maximum, and mean grain sizes were computed and expressed as mm and classed on the Udden-Wentworth scale with upper and lower divisions (Wentworth, 1922). The sorting was computed as the standard deviation and expressed as Ø and classed on Folk and Ward (1957) sorting scheme.

All the polished thin sections were reviewed using the conventional petrographic microscope for a detailed description of framework and diagenetic constitutes and pore system. The modal composition of framework and diagenetic constitutes and pores were quantified by counting 300 counts per thin section using an integrated electromechanical microscope stepping stage and a PETROG™ digital petrography software.

Four carefully selected thin sections have been subjected to a Quantitative Evaluation of Minerals examination using Scanning Electron Microscopy (QEMSCAN®). It is a computerized system that composes of a Quanta 650 FEG scanning electron microscope (SEM) coupled with two Energy-dispersive X-ray (EDX) spectroscopy detectors of Bruker. The QEMSCAN integrates the acquired backscattered images and X-ray data with an extensive mineral database to identify and quantify mineralogical phases. The main purpose of running a QEMSCAN examination is to understand and quantify the mineralogical distribution in each examined thin section. The selected thin sections were coated with carbon using Quorum EMS 150 R ES and subsequently were loaded into the QEMSCAN. The X-Ray beam operation conduction was generated by an accelerating voltage of 15 kV and current of 10 nA (±0.05). The field-scan mode was with different dimensions and point spacings, including areas of 6 mm^2, 3 mm^2, and 0.5 mm^2 and point spacings of 5, 2, and 0.5 μm, respectively. Acquiring and processing the QEMSCAN data were performed at the Center for Integrative Petroleum Research, King Fahd University of Petroleum and Minerals, Dhahran, Saudi Arabia.

Twenty representative sandstone samples were chosen and coated with gold prior to examination under a JEOL-scanning electron microscope (SEM) combined with a dispersed energy spectrometer (EDS). The samples were examined for the textural habits and paragenetic relations of various types of diagenetic minerals and porosity type and geometry. The samples were examined under a 20 kV and 4.5 × 10-11 A current beam of wavelength. The SEM and EDS analyses have been carried out at the Central Analytical and Applied Research Unit (CAARU) Laboratories of Sultan Qaboos University, Sultanate of Oman.

Twenty sandstone samples have been chosen and powdered (<200 mesh size) for X-Rays Diffraction (XRD) examination. The examination was performed to determine the structure of the sample contained minerals, especially clay minerals. The resultant XRD pattern has been analyzed and indexed using HighScore Plus Software. The XRD patterns were recorded on PANalytical X Pert PRO diffractometer using graphite filtered CuKα radiation (λ = 1.5405 °A) at 45 kV and 40 mA within a scanning rate of 0.2307/sec from 0° (start angel) to 70° (end angel). The XRD analysis was carried out at the Central Analytical and Applied Research Unit (CAARU) laboratories of Sultan Qaboos University, Sultanate of Oman.

Seven calcite and dolomite cemented sandstone samples have been chosen for oxygen- and carbon-isotope analysis to decipher the origin of pore water chemistry and temperatures at which the cement was precipitated. Oxygen- and carbon-isotope for each analyzed samples represents a prevailing carbonate cement type of that sample. Oxygen and carbon isotope results are designated in the δ notation and reported per mil (‰) relative to the Vienna Pee Dee Belemnite (V-PDB) and Standard Mean Ocean Water (SMOW) standards. The oxygen and carbon isotope analysis has been conducted at the Stable Isotope Laboratories within the School of Natural and Built Environment of the Queen's University of Belfast, Northern Ireland.

4. Results

4.1. Detrital constitute aspect

Texturally, the Barik Formation detrital constitute is predominantly subangular to subrounded and display a narrow range of grain size variants between coarse-grained silts to fine-grained sands (0.050.12 mm; av. 0.09 mm; Table 1 and Fig. 3A). It is classed as a moderate to very well-sorted (0.81–0.63; av. 0.74 mm; Table 1) reflecting fairly their textural maturity (Fig. 3B). There is no noticeable wide variant in sorting and grains size among the lithofacies association and parasequences (Figs. 3A and B).

Mineralogically, the detrital constitute is dominantly feldspathic-to subfeldspathic arenites in composition (sensu Folk, 1968, Fig. 4), reflecting relatively a mineralogical immaturity. There is no noticeable variant in mineral composition among the lithofacies association and parasequences (Table 1). The detrital grains are dominantly quartz (22.7–72.7; av. 52.8 vol%) and feldspars (8.3–34; av. 19.3 vol%), and rarely lithic fragments (0.0–4.0; av. 0.86 vol%), micas (0.0–8.7; av. 0.9 vol%), and heavy minerals (0.0–2.0; av. 0.2 vol%; Table 1). Among the detrital grains, monocrystalline quartz of a plutonic origin with a uniform and less undulate extension is the prime constituent (22.7–70.3; av. 49.6 vol%). Polycrystalline quartz with a sutured contact of low-grade metamorphic origin is significantly less abundant (0–10.7; av. 3.2 vol %). The potassic feldspars, orthoclase (4.0–28.7; av. 13.9 vol%), are more abundant than the plagioclase (1.3–7.0; av. 3.9 vol%). Most of the feldspar grains are altered, being either dissolved or replaced by kaolin

Table 1
A summary table presenting texture (i.e., grain size and sorting) and mineral composition and diagenetic alterations modal of the studied Barik Formation deposits in the Haushi-Huqf region of central Oman , grouped by facies associations. **Key: n=number of samples, Min=minimum, Max=maximum, Av=average, SD=standard deviation, csltU=coarse silt upper limit, vfsL=very fine sand lower limit, vfsU=very fine sand upper limit, vws=very well sorted, ws=well sorted, mws=moderately well sorted, IGC=intergranular cement, IPV=intergranular pore volume.**

Formation/Facies Association	Barik [n-152]				FA1 Mouth bar/shoreface [n=35]				FA2 Tidal flat [n=8]				FA3 Tidal channel [n=65]				FA4 Delta distributary channel [n=44]			
Statistics	Min	Max	Av	SD	Min	Max	Av	SD	Min	Max	Av	SD	Min	Max	Av	SD	Min	Max	Av	SD
Mean grain size (mm)	0.05	0.12	0.09	0.01	0.06	0.11	0.09	0.01	0.05	0.09	0.08	0.01	0.05	0.12	0.09	0.01	0.07	0.12	0.09	0.01
Mean grain size (cat)	csltU	vfsU	vfsU	-	csltU	vfsU	vfsU	-	csltU	vfsU	vfsL	-	csltU	vfsU	vfsU	-	vfsL	vfsU	vfsU	-
Sorting (Ø)	0.30	0.67	0.42	0.05	0.34	0.60	0.43	0.06	0.37	0.52	0.41	0.06	0.30	0.67	0.42	0.06	0.34	0.52	0.42	0.04
Sorting (mm)	0.81	0.63	0.74	0.96	0.79	0.66	0.74	0.96	0.77	0.70	0.76	0.96	0.81	0.63	0.75	0.96	0.79	0.70	0.75	0.97
Sorting (cat)	**vws**	**mws**	**ws**	-	**vws**	**mws**	**ws**	-	**ws**	**mws**	**ws**	-	**vws**	**mws**	**ws**	-	**vws**	**mws**	**ws**	-
Framework Grains	**53.33**	**89.67**	**74.23**	**6.36**	**53.33**	**89.33**	**74.89**	**8.52**	**66.00**	**87.67**	**75.39**	**8.13**	**60.00**	**89.67**	**73.45**	**5.86**	**63.00**	**85.67**	**74.67**	**4.51**
Quartz	22.67	72.67	52.82	7.37	41.33	70.33	54.92	8.55	43.33	60.00	50.67	6.24	22.67	72.67	52.52	8.00	41.33	68.67	52.23	5.16
Feldspar	8.33	34.00	19.28	4.44	8.33	29.00	17.93	4.96	13.00	28.67	22.17	5.40	12.67	34.00	19.18	4.15	9.67	31.33	20.11	3.99
Rock Fragment	0.00	4.00	0.86	0.72	0.00	3.33	0.66	0.73	0.33	1.33	0.83	0.35	0.00	2.33	0.83	0.62	0.00	4.00	1.10	0.84
Mica	0.00	8.67	0.87	1.30	0.00	4.33	1.10	1.24	0.00	8.67	1.44	3.03	0.00	6.33	0.64	1.01	0.00	3.67	0.60	0.79
Heavy Minerals	0.00	2.00	0.17	0.30	0.00	2.00	0.21	0.37	0.00	0.00	0.00	0.00	0.00	0.67	0.15	0.21	0.00	1.67	0.20	0.35
Accessory Grains	0.00	6.33	0.22	0.63	0.00	0.67	0.07	0.16	0.00	0.67	0.28	0.33	0.00	1.33	0.13	0.23	0.00	6.33	0.42	1.05
Matrix	0.00	0.00	0.00	0.00	0.00	0.00	0.00	0.00	0.00	0.00	0.00	0.00	0.00	0.00	0.00	0.00	0.00	0.00	0.00	0.00
Diagenetic Alterations	**0.00**	**36.33**	**4.36**	**5.06**	**0.00**	**36.33**	**5.96**	**7.68**	**0.00**	**16.33**	**2.44**	**5.30**	**0.00**	**18.67**	**3.83**	**4.15**	**0.00**	**14.00**	**3.68**	**2.87**
Smectite	0.00	2.00	0.25	0.43	0.00	0.67	0.14	0.23	0.00	1.67	0.33	0.62	0.00	1.67	0.23	0.41	0.00	2.00	0.31	0.51
Kaolinite	0.00	2.33	0.07	0.33	0.00	2.33	0.15	0.48	0.00	0.00	0.00	0.00	0.00	0.00	0.00	0.00	0.00	2.33	0.09	0.40
Illite	0.00	16.33	1.78	2.31	0.00	7.33	1.54	2.19	0.00	9.67	1.61	3.33	0.00	16.33	1.77	2.66	0.00	8.00	1.81	1.69
Chlorite	0.00	0.33	0.00	0.03	0.00	0.33	0.01	0.06	0.00	0.00	0.00	0.00	0.00	0.00	0.00	0.00	0.00	0.00	0.00	0.00
Feldspar overgrowths	0.00	2.33	0.11	0.32	0.00	1.67	0.11	0.37	0.00	0.67	0.11	0.24	0.00	2.33	0.15	0.37	0.00	1.00	0.07	0.20
Calcite	0.00	13.33	0.46	1.77	0.00	10.67	1.20	2.52	0.00	1.00	0.00	0.35	0.00	13.33	0.42	1.92	0.00	0.00	0.00	0.00
Dolomite	0.00	10.00	0.25	1.13	0.00	10.00	0.85	2.16	0.00	0.00	0.00	0.00	0.00	1.33	0.11	0.29	0.00	0.33	0.02	0.07
Gypsum	0.00	7.33	0.25	1.07	0.00	0.33	0.01	0.06	0.00	0.33	0.06	0.12	0.00	3.67	0.17	0.61	0.00	7.33	0.60	1.76
Silica and quartz overgrowths	0.00	8.67	0.46	1.14	0.00	3.33	0.49	0.81	0.00	1.00	0.22	0.36	0.00	8.67	0.45	1.33	0.00	7.00	0.49	1.20
Iron-oxide	0.00	17.67	0.31	1.55	0.00	17.67	0.95	3.01	0.00	0.33	0.06	0.15	0.00	0.67	0.06	0.17	0.00	2.67	0.17	0.51
Porosity	**4.67**	**30.67**	**21.41**	**5.54**	**4.67**	**26.67**	**19.15**	**6.07**	**11.00**	**30.67**	**22.17**	**7.23**	**6.00**	**30.67**	**22.72**	**5.49**	**12.33**	**30.00**	**21.65**	**4.30**
Primary	3.00	29.33	18.74	6.12	3.00	26.33	16.17	7.07	10.33	26.33	19.39	6.76	3.67	29.33	19.94	6.36	11.33	28.33	19.48	4.10
Secondary	0.00	11.67	2.67	2.34	0.00	10.67	2.98	2.94	0.67	6.00	2.78	1.77	0.00	11.67	2.78	2.43	0.00	7.67	2.17	1.65
Total frameworks	**53.33**	**89.67**	**74.23**	**6.36**	**53.33**	**89.33**	**74.89**	**8.52**	**66.00**	**87.67**	**75.39**	**8.13**	**60.00**	**89.67**	**73.45**	**5.86**	**63.00**	**85.67**	**74.67**	**4.51**
Total ductiles	**0.00**	**9.33**	**1.02**	**1.43**	**0.00**	**5.33**	**1.23**	**1.36**	**0.00**	**9.33**	**1.50**	**3.22**	**0.00**	**8.00**	**0.77**	**1.22**	**0.00**	**3.67**	**0.78**	**0.86**
Total authigenics	**0.00**	**36.33**	**4.36**	**5.06**	**0.00**	**36.33**	**5.96**	**7.68**	**0.00**	**16.33**	**2.44**	**5.30**	**0.00**	**18.67**	**3.83**	**4.15**	**0.00**	**14.00**	**3.68**	**2.87**
Total cements (IGC)	**0.00**	**36.33**	**4.15**	**4.71**	**0.00**	**36.33**	**5.60**	**7.08**	**0.00**	**16.33**	**2.44**	**5.30**	**0.00**	**18.67**	**3.53**	**3.79**	**0.00**	**14.00**	**3.67**	**2.87**
Total grains replacives	**0.00**	**7.33**	**0.76**	**0.97**	**0.00**	**7.33**	**0.54**	**1.30**	**0.00**	**2.67**	**0.67**	**1.08**	**0.00**	**2.67**	**0.65**	**0.68**	**0.00**	**4.00**	**1.02**	**0.91**
IPV excluding clays	**7.00**	**45.67**	**22.89**	**7.04**	**8.67**	**45.67**	**21.77**	**10.07**	**11.67**	**29.67**	**21.83**	**7.16**	**7.00**	**38.33**	**23.47**	**6.64**	**13.33**	**31.33**	**23.14**	**4.17**
IPV including clays	**7.00**	**45.67**	**22.89**	**7.04**	**8.67**	**45.67**	**21.77**	**10.07**	**11.67**	**29.67**	**21.83**	**7.16**	**7.00**	**38.33**	**23.47**	**6.64**	**13.33**	**31.33**	**23.14**	**4.17**

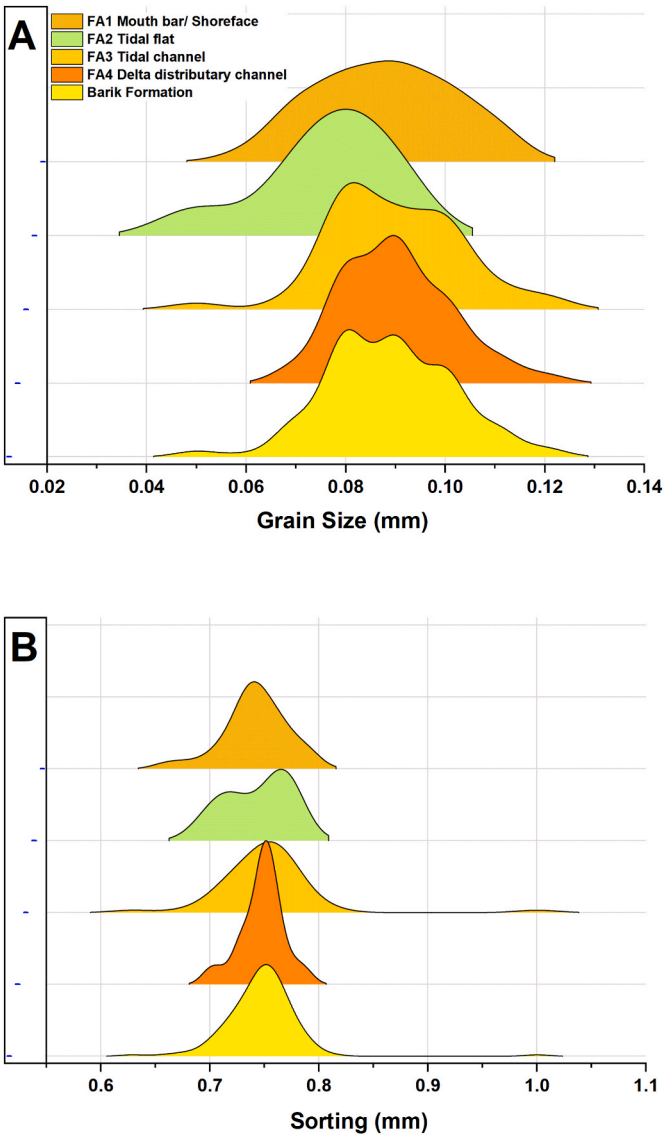

Fig. 3. A ridgeline chart showing (A) the mean grain size and (B) mean sorting of the Barik Formation sandstones and siltstones amongst all facies associations.

and albite. Lithic fragments are rare and mostly sedimentary in origin (0.0–4; av. 0.9 vol%) including sandstones, mudstone, and chert grains. Mica is also rare and including biotite and muscovite (0–5.0; av. 0.6 vol %; 0–4.0; av. 0.3 vol%; respectively). Some of the micas are altered and replaced by kaolin. Heavy minerals are rare including zircon and rutile. The matrix is not abundant (0.0–6.3; av. 0.2 vol%).

4.2. Diagenetic alterations aspect

Theassessment of the Barik Formation siltstones and sandstones using petrographic and geochemical techniques has revealed to some extent a mildly heterogeneous distribution of diagenetic processes and products across various depositional facies, parasequences, and paleo-burial depths. These diagenetic processes have led to alterations in the detrital composition through dissolution and replacement, and have impacted theevolution and distribution of reservoir porosity through dissolution, replacement, and compaction. These diagenetic processes and products include thepresence of mechanically infiltrated clays (i.e., smectite), the transformation of feldspars, micas, and precursor clays into kaolinite, illite, and chlorite, cementation by calcite, dolomite, silica, quartz and feldspar overgrowths, Fe-oxides, and sulfates and dissolution of feldspars and micas (i.e., chemically unstable grains), as well as mechanical and chemical compaction.

4.2.1. Smectite

Smectite (0.0–2.0%; av. 0.3 vol%; Table 1) in the studied samples occur as a continuous cover (1–3 μm thick) coating the surface and at the contact between detrital grains (i.e. feldspar and quartz). The smectite, under the polarized and cross-polarized light (PPL and XPL) microscope, appears as a colorless and light-yellow interference color respectively (Figs. 5A and B). The SEM investigations showed that smectite has a honeycomb and platelet-like textures with a perpendicular alignment on the surface of detrital grains (i.e., feldspar and quartz; Fig. 5C). As showed by EDS results (Fig. 5D), smectite encompasses substantial amounts of oxygen (52.6 wt%), silica (19.9 wt%), aluminum (14.6 wt %), magnesium (0.3 wt%), sodium (0.6 wt%) and calcium (2.6 wt%). The bulk XRD of the analyzed samples indicates the existence of smectite (Fig. 6). Textural relationships revealed that smectite is engulfed by feldspar and quartz overgrowths. Smectite is mostly encountered in the delta distributary channel, tidal channel, and tidal flat and infrequently encountered in the mouth-bar/shoreface facies association sandstones, notably within the mouth bar.

4.2.2. Kaolinite

Kaolinite (0.0–2.3; av. 0.1 vol%; Table 1; Figs. 7A–G) occurs as an aggregates of micro-scale crystals of <4 μm thick with a whitish color under the plane-polarized light (PPL; Figs. 7A and C) and greyish interference color under cross-polarized light (XPL; Figs. 7B and D) microscope, replacing detrital grains and filling intergranular and intragranular pores. However, the authigenic kaolinite is commonly replacing incompletely to completely the detrital feldspars and infrequently micas, mud intraclasts, and mud matrix (Figs. 7A–G). The optical microscope and SEM examinations revealed that the incompletely kaolinitized feldspars contain detrital feldspar grains remains (Fig. 7E). The completely kaolinitized feldspars are small-sized scattered patches resembling detrital feldspar grains' size and outline. Moreover, the SEM examination showed that the complete kaolinitized feldspar grains are outlined by chlorite and illite clays. In some cases, kaolinite crystals partially fill moldic pores of dissolved detrital feldspars that are coated with illite and chlorite clays. Under the optical microscope, kaolinitized micas display an expanded textural habit inflating towards the nearby pore space (Figs. 7A and B). Kaolinitized mud intraclasts are observed as scattered patches of large-sized (ca. 500 μm; Figs. 7C and D) irregular clast shapes that are pressed between the firm grains tending to plug the nearby intergranular pores (Fig. 7F). The outline of the thinnest kaolinite crystals, in some cases, displays the growth of fibrous illite crystals (Fig. 7G).

The EDS showed that kaolinite comprises substantial amounts of oxygen (30.2 wt%), silica (25.3 wt%), and aluminum (20.5 wt%) (Fig. 7H). Bulk XRD results of the analyzed samples support the existence of kaolinite (Fig. 6). There is an insignificant variant of kaolinite amounts in relation to depositional facies and among parasequences. However, kaolinite is observed in the delta distributary channel and the mouth bar/shoreface facies association, while the kaolinite in the rest of the facies associations is rarely found.

4.2.3. Illite

Illite (0.0–16.3%; av. 1.8 vol%; Table 1; Figs. 8A–E) occurs predominantly as coats enveloping grains and rarely as bridging pores and less commonly as illitized kaolinite crystals and illitized micas and feldspars. The Illite coating grains, under the cross-polarized light (XPL) microscope, appear as a yellow interference color (Fig. 8A). The Illite coatings are tangential aligned rims with variable thicknesses ranging between 2 and 5 μm around and also at the contact between detrital grains (i.e. quartz and feldspar; Fig. 8A). Additionally, the illite fills the depression puts on the detrital grains surface. The SEM examinations demonstrate that the illite rims are characterized by honeycombs and

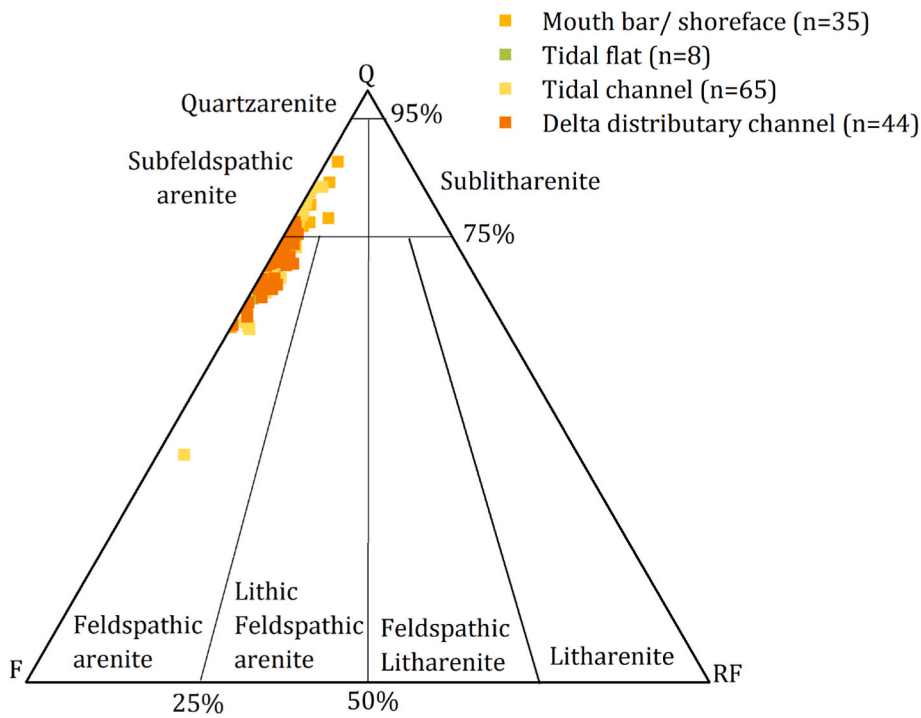

Fig. 4. Detrital composition of Barik Formation plotted in a Folk (1968) ternary diagram illustrating that it is primarily feldspathic- and subfeldspathic arenite.

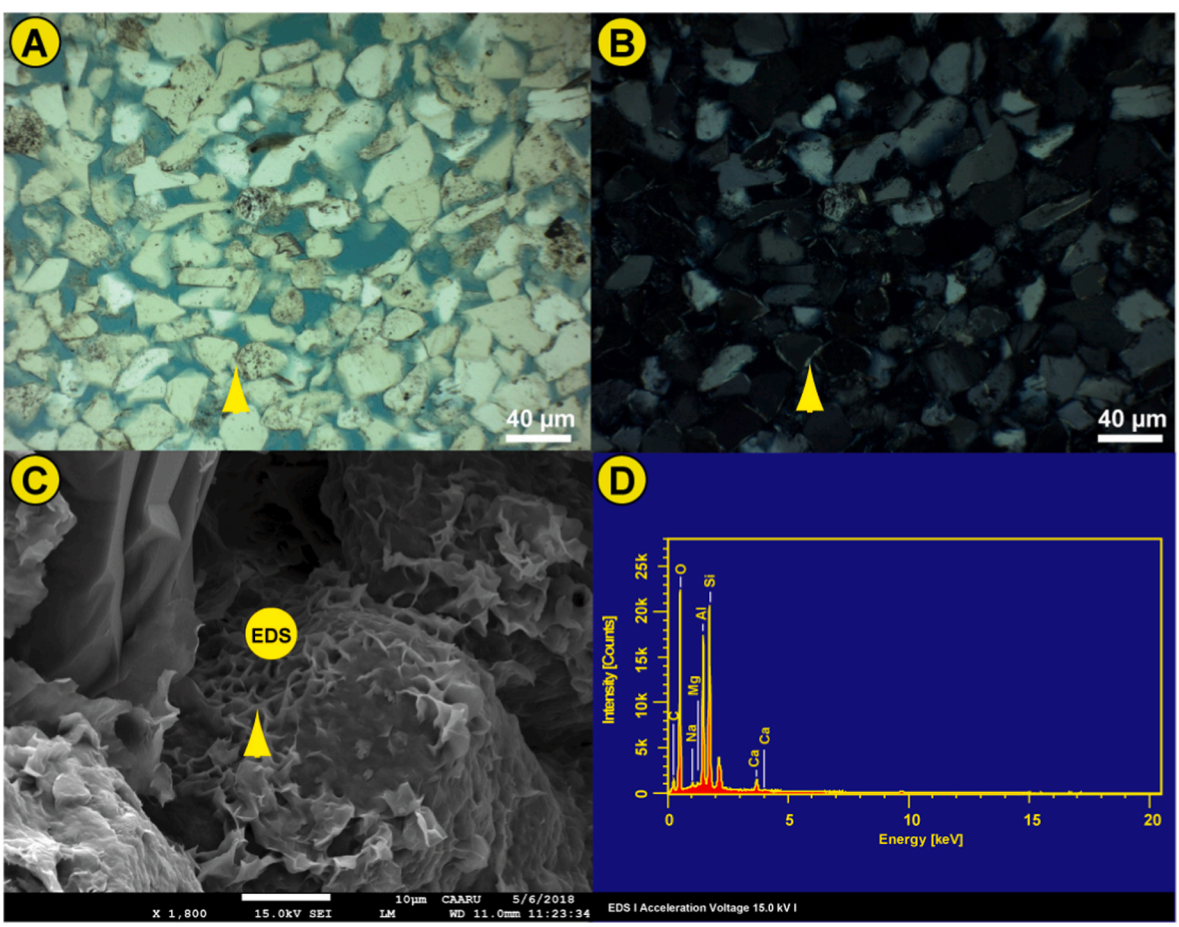

Fig. 5. Photomicrograph showing (A and B) a colorless and yellowish-color smectite enveloping detrital quartz grains (PPL and XPL; respectively) (yellow arrow), (C) SEM image showing a honeycomb texture (yellow arrow), and (D) EDS spectrum showing the major elements of smectite clay (Na, Mg, Ca, Al, Si, O).

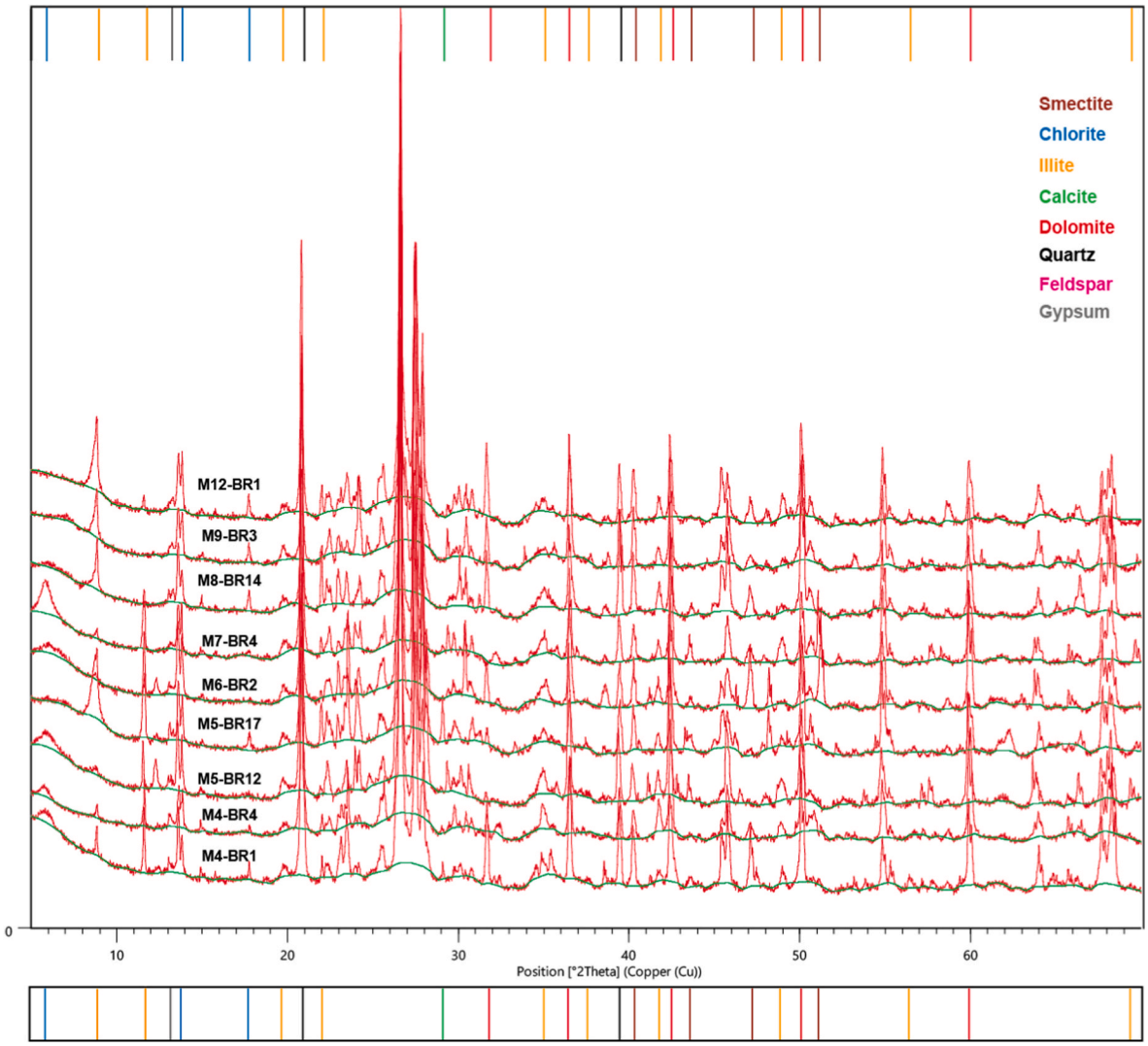

Fig. 6. XRD spectrum of a representative samples from the Barik Formation showing the presence of smectite, chlorite, illite, calcite, dolomite, quartz, feldspar, and gypsum.

cornflakes texture with filamentous termination (Figs. 8B–D). The Illite rims that coat grains commonly occur as a continuous and, in some case, as discontinuous cover around the entire surface of quartz and feldspar grains (Fig. 8A). Illitic bridging pores are rare and bond the passageways between detrital grains. Illititized kaolinite displays a fibrous texture lining the outline of the kaolinite crystals (Fig. 8E). Illitized micas and feldspars display a growth of fibrous illite crystals. Textural relationship revealed that the illite is engulfed by quartz and feldspar overgrowths, and the illitized kaolinite engulfs the quartz and feldspar overgrowths (Fig. 8D).

EDS results of the analyzed samples showed significant amounts of oxygen (45.5 wt%), aluminum (5.8 wt%), silica (15.7 wt%), potassium (2.3 wt%), and sodium (2.1 wt%) (Fig. 8F). Bulk XRD results of the analyzed samples also support the existence of illite (Fig. 6). The Illite coating grains are relatively common in all facies associations.

4.2.4. Chlorite

Chlorite (0.0–0.3%; av. 0.003 vol%; Table 1; Figs. 9A–E) occurs as a coating grain with greyish interference colors under the cross-polarized light (XPL; Fig. 9A) and a light green color under the plane-polarized light microscope (PPL) microscope. The Chlorite coating grains is represented by a continuous envelop (1–3 μm thick) covering the surfaces and at the contact between the detrital grains (Fig. 9A; i.e. quartz and feldspar). Under the SEM, the chlorite clays showed honeycomb and platelet-like textures that are aligned perpendicularly on the surfaces of quartz and feldspar grains (Figs. 9B and C).

The EDS results of the analyzed samples have significant amounts of oxygen (48.4 wt%), silica (16.3 wt%), aluminum (8.5 wt%), iron (5.0 wt %), magnesium (2.1 wt%), and variable amounts of potassium (1.6 wt%) (Fig. 9F). The Bulk XRD results showed that the analyzed samples contain chlorite (Fig. 6). Textural relationships revealed that the chlorite is engulfed by feldspar and quartz overgrowth (Figs. 9D and E). The Chlorite coating clays are occasionally detected in the mouth-bar/shoreface, notably within the mouth bar, thus being less abundant than illite grain-coating clays. Nevertheless, chlorite is found in trace amounts in the rest of facies associations.

4.2.5. Silica

Silica (0.0–8.7%; av. 0.5 vol%; Table 1; Figs. 10A–F), in the studied samples, is largely syntaxial quartz overgrowths and intergranular pore-filling forming concretions. The syntaxial quartz overgrowths (ca. 30–50 μm thick) occur as smooth euhedral crystals that cover either partially to entirely detrital quartz grains (Figs. 10A and B). Optical microscopic investigations showed, in a few cases, that the contact between the quartz grains and overgrowths is labeled by the existence of a yellow-colored illite. The SEM analyses provide additional evidence of

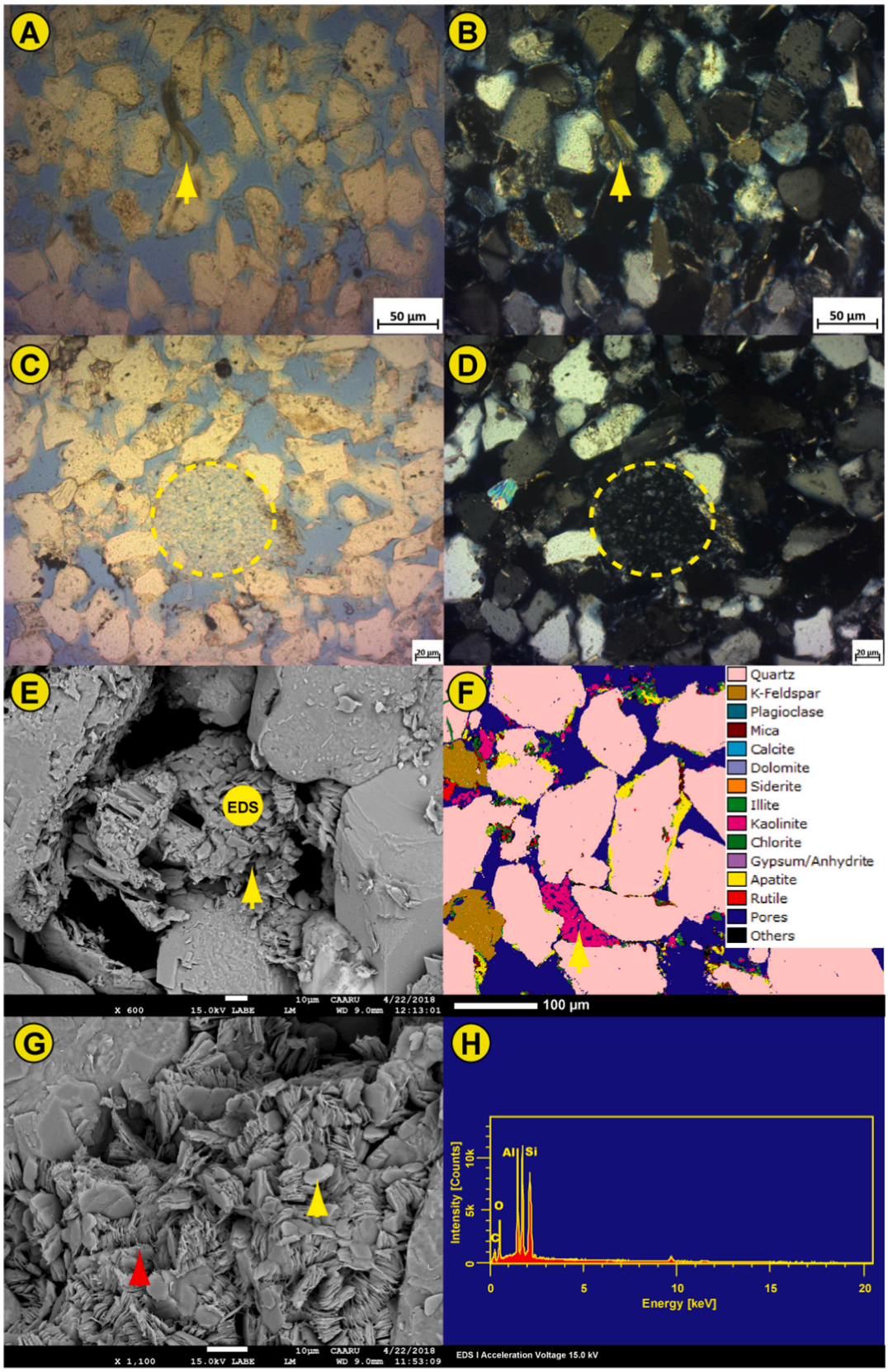

Fig. 7. Photomicrograph showing (A and B) the expanded texture of micas that are inflating towards the porespace with a whitish and gray interference color of kaolinite (PPL and XPL; respectively) (yellow arrow), (C and D) kaolinitized mudclast with a whitish and gray colors (PPL and XPL; respectively), (E) SEM image showing a partial kaolinitized feldspar (yellow arrow), (F) QEMScan image showing kaolinitized deformed mudclast (yellow arrow), (G) SEM image showing kaolinitized matrix (yellow arrow) and illitized kaolinite depicting fibrous crystals (red arrow), and (H) EDS spectrum showing the major elements of kaolinite clay (Al, Si, O).

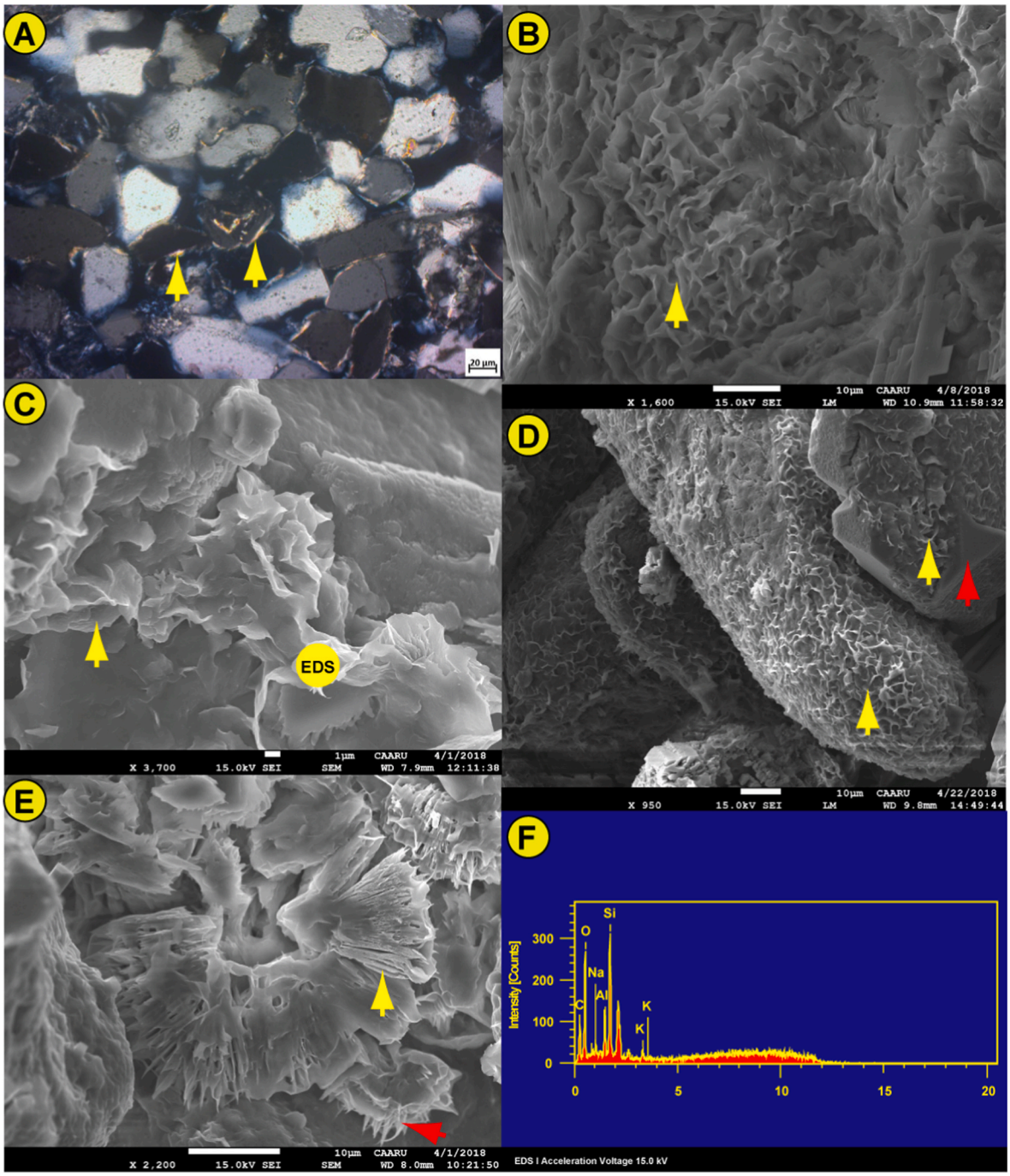

Fig. 8. Photomicrograph showing (A) yellow interference color of illite clay (yellow arrow), (B) SEM image showing a preserved honeycomb texture of illite clays with spiny termination (yellow arrow), (C) SEM image showing flakes like texture with spiny termination of illite clays (yellow arrow), (D) SEM image showing illite (yellow arrow) coated with quartz overgrowths (red arrow), (E) SEM image showing kaolinite (yellow arrow) that is subjected to illitization; spiny termination of illite crystals (red arrow), and (F) EDS spectrum showing the major elements of illite clay (Na, K, Al, Si, O).

the existence of illite and chlorite clays at the contact between the quartz and feldspar grains surfaces and overgrowths. The SEM analysis also showed the growth of microscopic quartz crystals in the spaces between the chlorite platelets, but these microscopic quartz crystals ultimately merged together to form larger quartz crystals (Figs. 10C and D). Syntaxial quartz overgrowth is observed in all lithofacies associations being common in the delta distributary channel, tidal channel, and mouth bar/shoreface in comparison with tidal flat facies association.

Silica occurs also as scattered patches forming small-sized concretions of ca. 0.5 cm (Figs. 10E and F). The silica in concretions fills intergranular pores and encloses grains forming poikilotopic textures in relatively uncompacted grains. Silica concretion is most common in the delta distributary channel and tidal channel facies associations and is less common in the mouth bar/shoreface and tidal flat facies associations.

4.2.6. *Feldspar*

Authigenic feldspar occurs commonly in the form of overgrowth and traces of albitization of detrital feldspar grains (0.0–2.3%; av. 0.1 vol%; Table 1; Figs. 11A–E). The SEM examinations showed that the authigenic feldspar overgrowth is characterized by smooth and euhedral rims covering partially to completely detrital K-feldspar grain with a

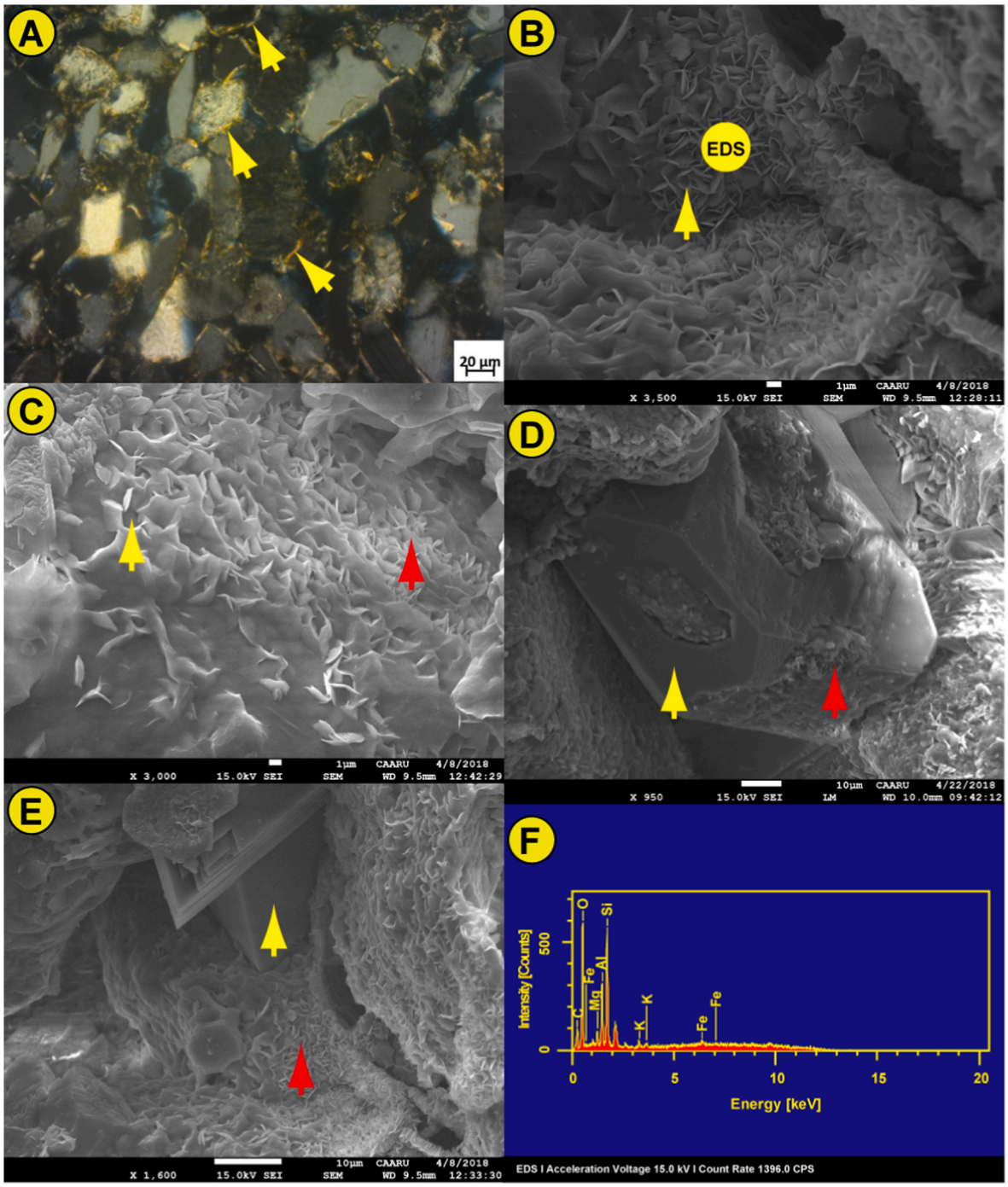

Fig. 9. Photomicrograph showing (A) yellow to greenish interference color of chlorite clay (yellow arrow), (B) SEM image showing a roselet texture of chlorite clays (yellow arrow), (C) SEM image showing weakly preserved honeycomb texture of chlorite (yellow arrow) that developed to a roselet texture (red arrow), (D) SEM image showing chlorite (red arrow) engulfed by quartz overgrowths (yellow arrow), (E) SEM image showing chlorite (red arrow) engulfed by feldspar overgrowths (yellow arrow), and (F) EDS spectrum showing the major elements of chlorite clay (Fe, Mg, K, Al, Si, O).

thickness of ca. 10–50 µm (Fig. 11A). The SEM investigations also showed that feldspar overgrowths are also composed of numerous rhombic euhedral crystals that grew on detrital K-feldspar grains (Fig. 11B). The rhombic euhedral crystals vary widely in size between 5 µm and 300 µm. The adjacent rhombic euhedral crystals, in many cases, merge and form large size crystals covering broad areas of feldspar grain surface (Figs. 11 B and C). The EDS examination revealed that the rhombic euhedral crystals of the feldspar overgrowths are predominantly potassium-rich that are marked by the existence of a significant amount of oxygen (47.1 wt%), silica (19.4 wt%), aluminum (6.7 wt%), and potassium (5.8 wt%) (Fig. 11F). Textural relationships revealed that the rhombic euhedral crystals are enclosed by and thus postdated illite and chlorite clays (Fig. 11D).

Albitization of feldspars occurs as aggregates of micro-sized albite crystals replacing K-feldspar grains (Fig. 11E). Albitization is usually associated with partially dissolved K-feldspar grains (Fig. 11E). The authigenic feldspar is similarly distributed within all facies associations.

4.2.7. Calcite

Calcite (0.0–13.3%; vol. 0.5%; Table 1; Figs. 12A–C) occurs as small-

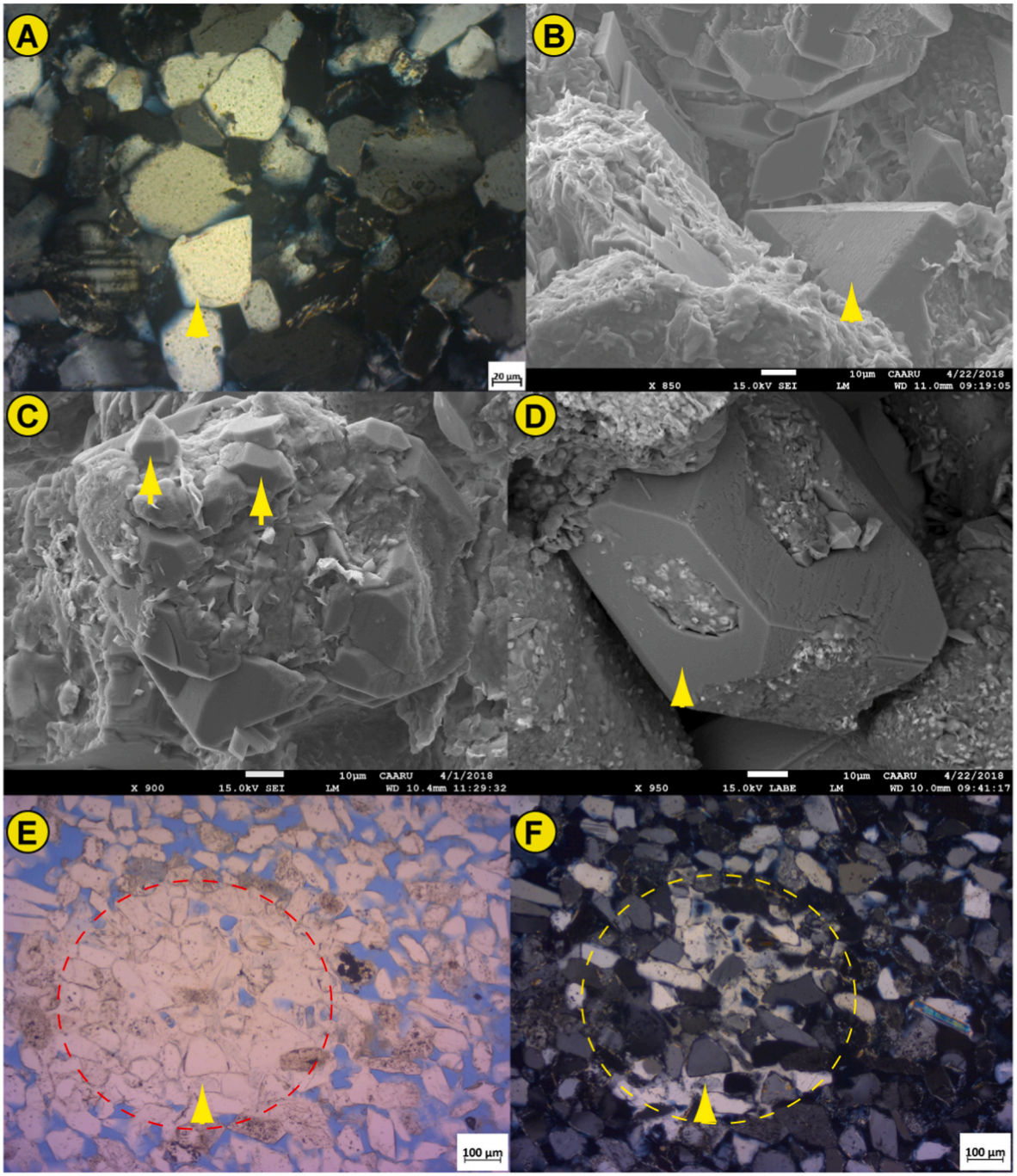

Fig. 10. Photomicrograph showing (A) well-developed quartz overgrowths around detrital quartz grain (XPL; yellow arrow), (B) SEM image showing typical hexagonal crystal of quartz overgrowths, (C) SEM image showing the development of micro-sized quartz crystals that are eventually merge to form large-sized quartz crystals (yellow arrow), (D) SEM image showing the growths of quartz overgrowth and engulfment of chlorite clays (yellow arrow), and (E and D) photomicrography showing the development of micro-sized silica concretions in which the silica is filling relatively closely packed framework grains (yellow arrow).

sized concerations and scattered patches that is represented by a blocky and poikilotopic intergranular pore-filling cement in fairly uncompacted framework grains (i.e., large-sized pores; 150–200 µm) and also appears to fill small-sized pores in compactly framework grains (i.e., small-sized pores; 50–100 µm) (Figs. 12A and B). The textural relationship, in some cases, revealed that calcite cement filling small-sized pores is postdating quartz overgrowths (Fig. 12C). The bulk XRD results of the studied samples verifies the occurrence of calcite. Oxygen and carbon isotopic signatures of sandstone samples that are mostly cemented by blocky and poikilotopic calcite filling intergranular pores in uncompacted framework grains displayed a modest range of $\delta^{18}O_{VPDB}$ values between −9.05‰ and −5.54‰ and a narrow range of $\delta^{13}C_{VPDB}$ values between −4.36‰ and −2.26‰ (Table 2; Fig. 13). Thus, the reported $\delta^{18}O_{VPDB}$ and $\delta^{13}C_{VPDB}$ values are not representative for the calcite that fills small-sized pores and postdating quartz overgrowths. Calcite cement is most common within mouth-bar/shoreface and tidal channel facies association and rarely noticeable within the tidal flat facies association and absent in delta distributary channel facies association.

4.2.8. Dolomite

Dolomite (0.0–10%; av. 0.3 vol%; Table 1; Figs. 14A–D) is observed as scattered non-ferroan small rhombic crystals, which are 10–50 m in

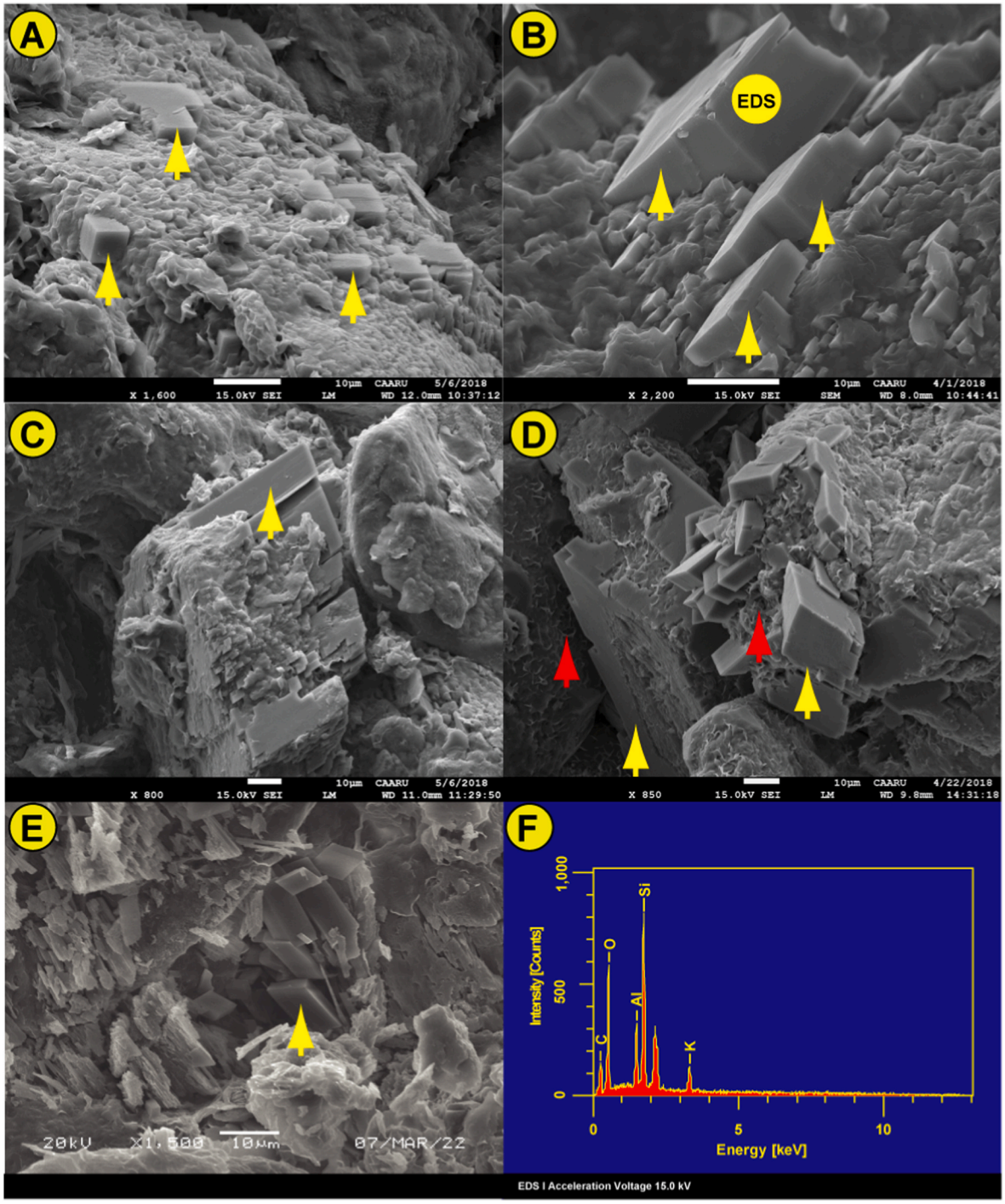

Fig. 11. SEM image showing (A) well-developed micro-sized scattered crystals of feldspars on a detrital feldspar grain forming a feldspar overgrowths (yellow arrow), (B) SEM image (large view) showing typical crystal shape of feldspar overgrowths (yellow arrow), (C) SEM image showing the development of large-sized feldspar crystals (yellow arrow), (D) SEM image showing the growths of feldspar overgrowth (yellow arrow) and engulfment of chlorite clays (red arrow), (E) SEM image showing the development of micro-sized albite crystals (yellow arrow), and (F) EDS spectrum showing the major elements of feldspar overgrowth (K, Al, Si, O).

size. These crystals typically fill fairly large pores (200–400 μm) in uncompacted grains and also smaller pores (10–50 μm) in compactly grains (Figs. 14A–C). In some cases, dolomite postdates quartz overgrowths (Fig. 14D). The bulk XRD analysis approves the existence of dolomite (Fig. 6). Oxygen and carbon isotope signatures of sandstone samples predominantly cemented by dolomite that fills fairly large pores in uncompacted framework grains displayed a fairly narrow range of $\delta^{18}O_{VPDB}$ values between −8.63‰ and −5.95‰ and $\delta^{13}C_{VPDB}$ values between −4.37‰ and −1.87‰ (Table 2; Fig. 13). Thus, the reported $\delta^{18}O_{VPDB}$ and $\delta^{13}C_{VPDB}$ values are not representative for the dolomite that fills small-sized pores and postdating quartz overgrowths. Dolomite cement is most common within the mouth bar/shoreface, rarely noticeable within tidal channel and delta distribuary channel facies associations and absent in the tidal flat facies association.

4.2.9. Gypsum

Gypsum is a minor diagenetic constituent. The gypsum occurs as aggregates of small-sized tabular and elongated crystals (10–50 μm) and

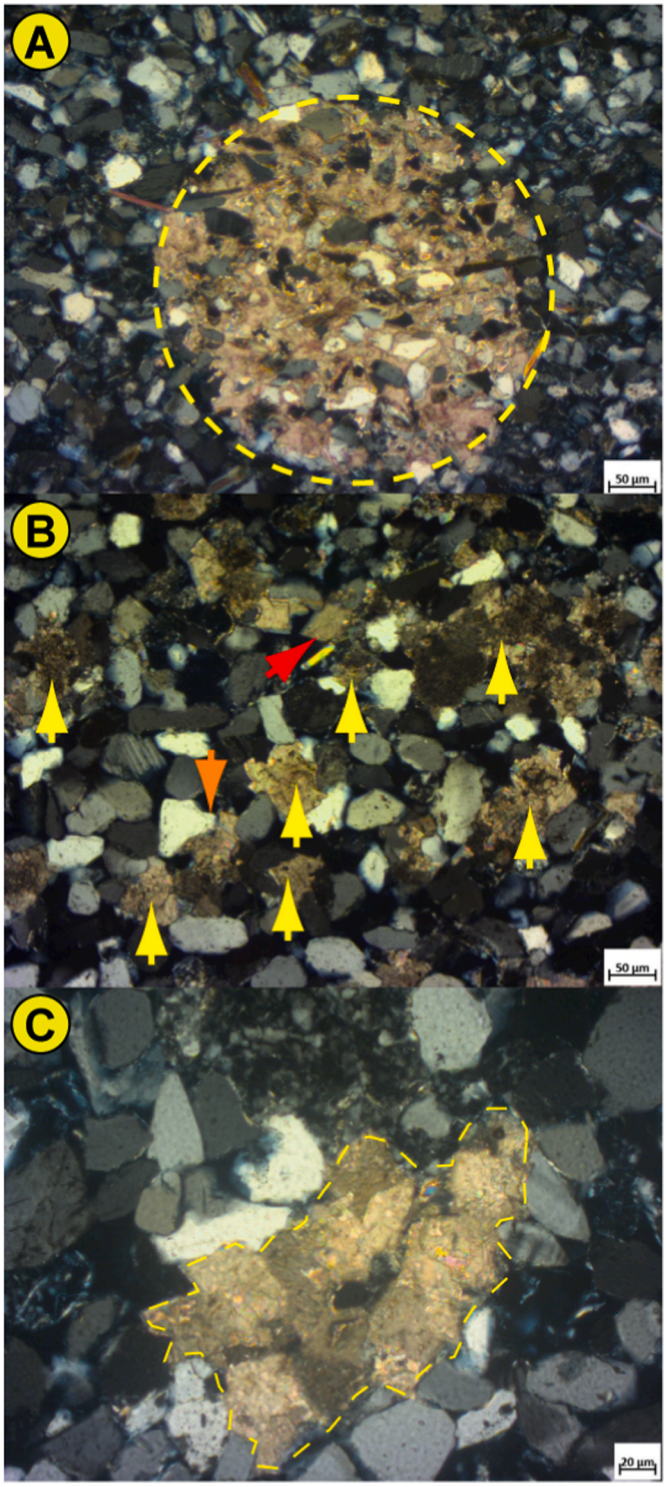

Fig. 12. Photomicrograph showing (A) micro-sized concretion of calcite characterized by blocky and poikilotopic intergranular pore-filling texture in a relatively loosely packed framework grains (XPL), (B) blocky intergranular pore-filling texture of calcite in relatively loosely packed framework grains (yellow arrow) and in tightly packed framework grains (red arrow) engulfing quartz overgrowths (orange arrow) (XPL), and (C) blocky texture of calcite filling intergrowthal pores in loosely packed framework grains.

filling small-sized intergranular pores in compactly grains (10–100 µm) (Figs. 15A and B). The bulk XRD results of the analyzed rock samples supports the existence of gypsum (Fig. 6). Gypsum is most common within the delta distributary channel and tidal channel facies

Table 2
A summary table presenting the stable O- and C-isotope values for diagenetic calcite- and dolomite-cemented samples from the Barik Formation outcrops in the Haushi-Huqf region of central Oman.

Calcite			Dolomite		
Sample N°	$\delta^{13}C_{VPDB}$‰	$\delta^{18}O_{VPDB}$‰	Sample N°	$\delta^{13}C_{VPDB}$‰	$\delta^{18}O_{VPDB}$)
M10 Br 1	−3.57	−6.25	M10 Br 1	−4.24	−8.63
M10 Br 2	−3.13	−5.54	M10 Br 2	−3.99	−7.7
M10 Br 4	−3.04	−6.8	M10 Br 4	−2.24	−5.95
M10 Br 8	−2.26	−6.5	M10 Br 8	−2.73	−7.16
M10 Br 12	−2.76	−9.05	M10 Br 12	−1.87	−7.69
M10 Br 13	−3.19	−6.21	M10 Br 13	−4.15	−7.7
M10 Br 20	−4.36	−6.49	M10 Br 20	−4.37	−8.14

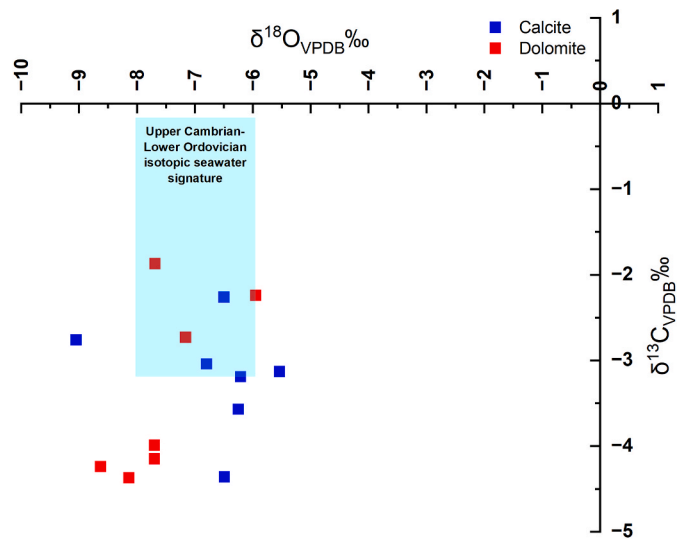

Fig. 13. Stable oxygen and carbon isotopes cross plot of seven calcite- and dolomite-cemented samples of the Barik Formation.

associations and rarely noticeable within other facies associations.

4.2.10. Fe-oxide

Fe-oxide (0.0–17.7%; av. 0.3 vol%; Table 1; Figs. 16A and B) is observed in the studied siltstone and sandstone samples, forming brown to black colored irregular coats around thedetrital grains (Fig. 16A). However, Fe-oxides sometimes are mixed with clays that coat the detrital grains (Figs. 16A and B). Fe-oxides are most common within the mouth bar/shoreface facies association and less common within the other facies associations.

4.2.11. Compaction

The optical microscopic and SEM examinations demonstrated that the studied siltstones and sandstones had undergone varied degrees of mechanical and chemical compaction. Mechanical compaction is proven by the developing point-to-point grains contact, pseudoplastic bending of micas and of mud intraclasts resulting in pseudomatrix formation (Figs. 17A and B). The SEM examinations revealed the rearrangement and closed packing of authigenic kaolinite crystals between compactly grains. On the other hand, chemical compaction is demonstrated by the presence of local intergranular pressure dissolution and thus formation of straight and concave-convex contacts between the feldspar grains as well as quartz grains (Figs. 17A and B). The chemical compaction is prevalent in the sandstones that lack early cementation and where illitic and chloritic clays are present along the interface of quartz grain contacts.

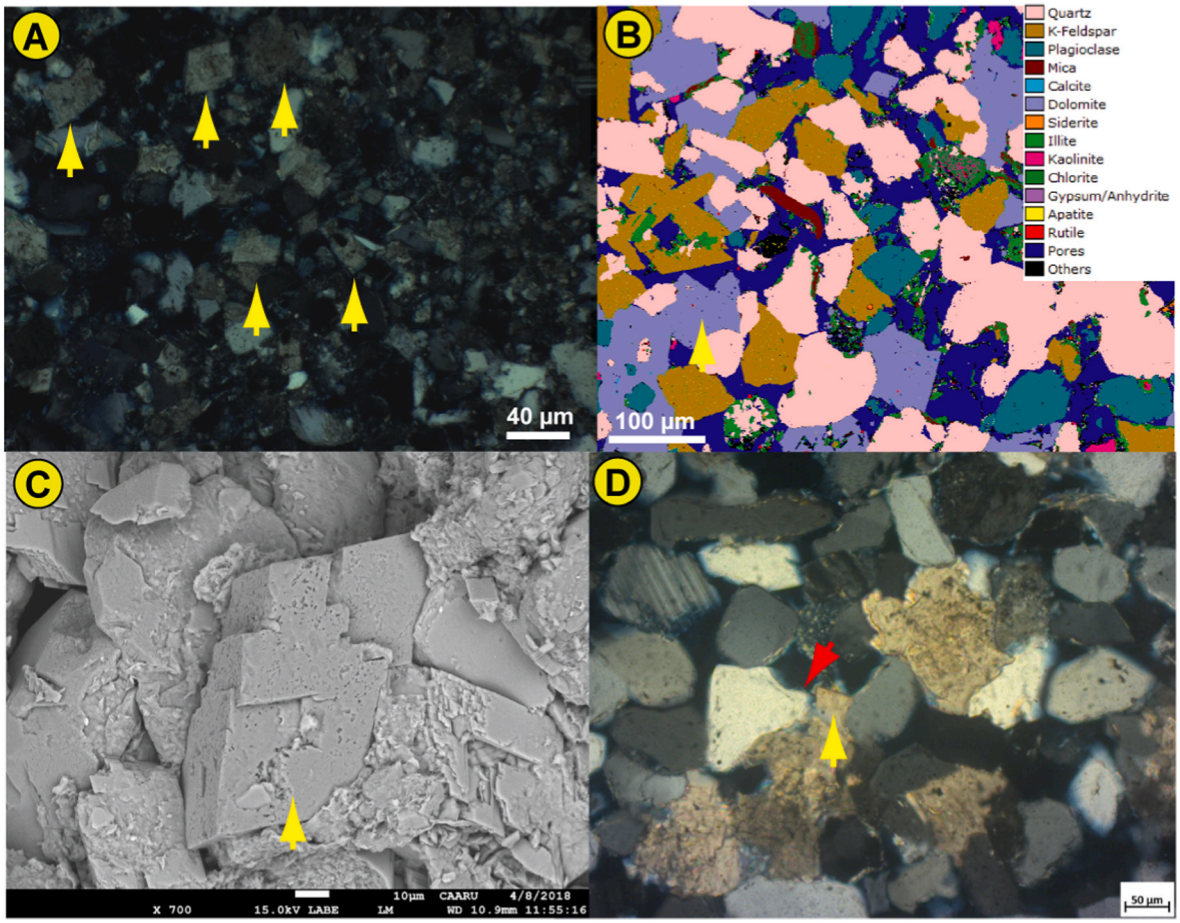

Fig. 14. Photomicrograph showing (A) the development of aggregates of rhombic crystals of dolomite filling intergranular pores in a relatively loosely packed framework grains (XPL; yellow arrows), (B) QEMScan showing aggregates of rhombic crystals of dolomite filling intergranular pores in a relatively loosely packed framework grains (XPL; yellow arrow), (C) SEM image showing typical rhombic crystal texture of dolomite (yellow arrow), and (D) photomicrograph showing rhombic dolomite filling small-sized intergranular pores (yellow arrow) engulfing quartz overgrowth (red arrow).

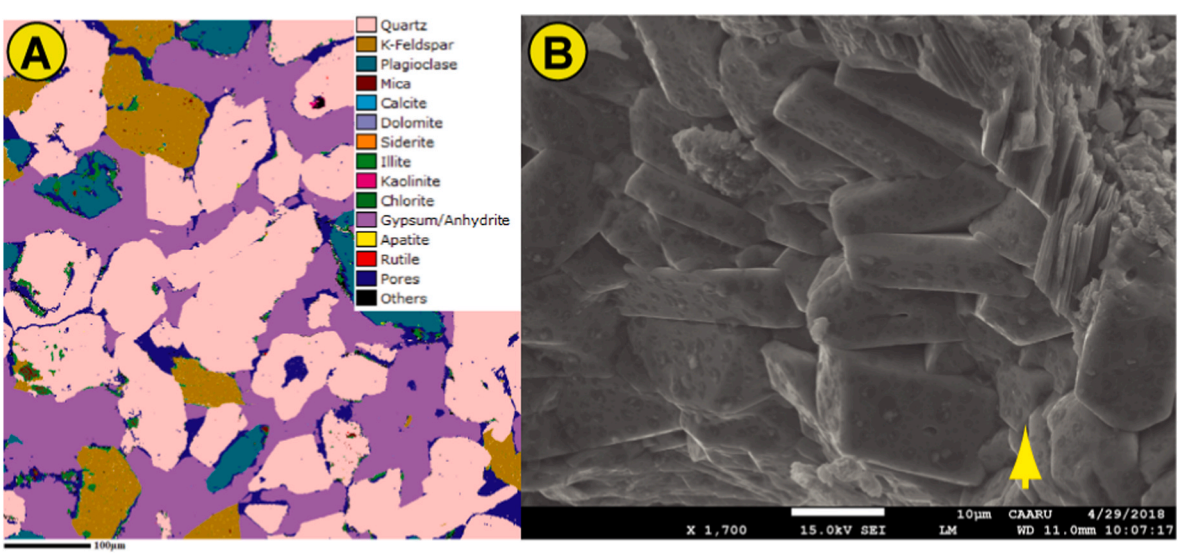

Fig. 15. QEMScan image showing (A) the development of intergranular pore-filling gypsum, and (B) SEM image showing well-developed tabular and prismatic crystals up to 200 µm in size of gypsum (yellow arrow).

4.2.12. Dissolution

The optical microscopic and SEM observations documented that the studied siltstones and sandstones have suffered considerable degrees of dissolution (0.0–28%; av. 2.7 vol%; Table 1; Figs. 18A–F). Dissolution is abundant in grains; feldspars and micas and matrix (Figs. 18A and B), and less commonly in cements; calcite and dolomite. The dissolved

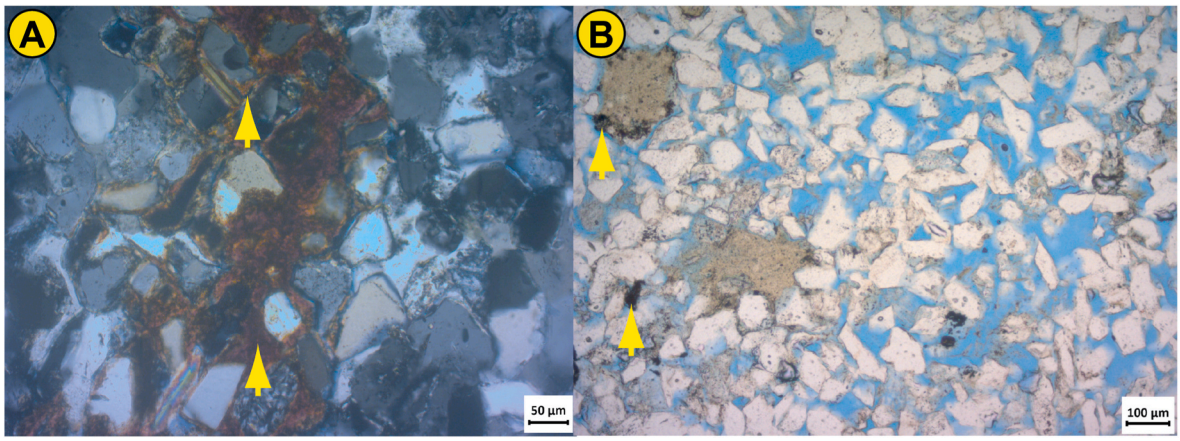

Fig. 16. Photomicrograph showing (A) brown to blackish-brown iron-oxide staining mud matrix and grain-coating clays (yellow arrows) (XPL), and (B) scattered black iron-oxide spots in mud matrix and scattered within porespace (yellow arrows) (PPL).

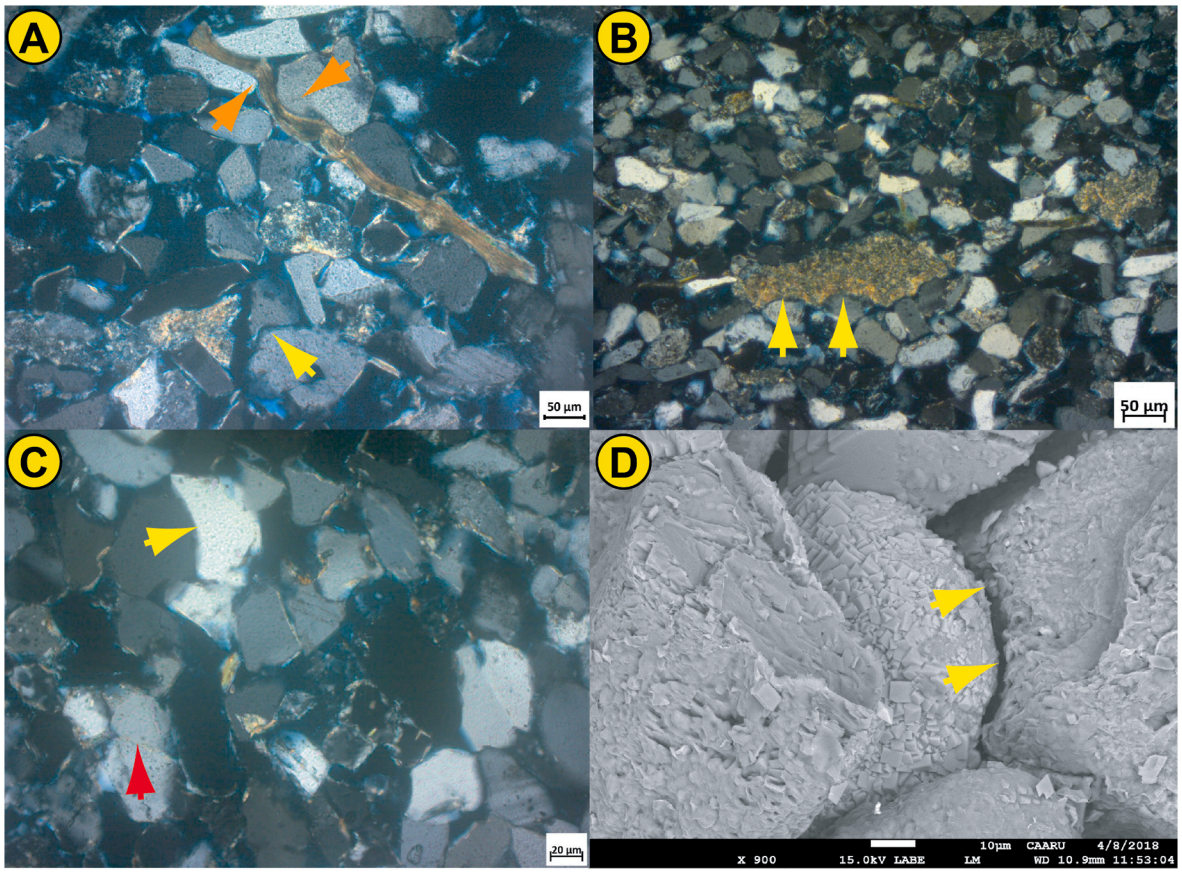

Fig. 17. Photomicrograph showing various degrees of mechanical and chemical compaction: (A) deformation of mica (orange arrows) and concave-convex grain contact (yellow arrows) (XPL), (B) deformation of mudclast and formation of pseudomatrix (yellow arrows) (XPL), (C) concave-convex (yellow arrow) and straight grain contact (red arrow) (XPL), and (D) SEM image showing the development of concave-convex grain contact (yellow arrows).

feldspars are commonly K-feldspars and plagioclase grains. In most cases, K-feldspars and plagioclase grains display different dissolution grades, from leaching to intense dissolution, creating micro- and macro-intragranular pores (Figs. 18C–F). The wholly dissolved feldspar grains are also documented, forming moldic pores (Fig. 18F). In addition, merged several-dissolved feldspar grains occur in the studied sandstones creating large outsized pores. Dissolved matrix results in enlarging the intergranular pores. Dissolution is common in all facies associations.

4.3. Porosity type and distribution aspect

The modal composition analysis reveals that the thin-section total porosity in siltstones and sandstones of the Barik Formation typically comprises primary and secondary pore types, including intergranular, intragranular, moldic, and intercrystalline pores (Table 1; Figs. 19A–F). The primary intergranular porosity encompasses a wide range of both macro- and micro-sized pores (100–1000 µm and <20 µm, respectively; Figs. 19A–F). The macro-sized intergranular pores are predominant and represent those pores that have survived the effects of compaction and/

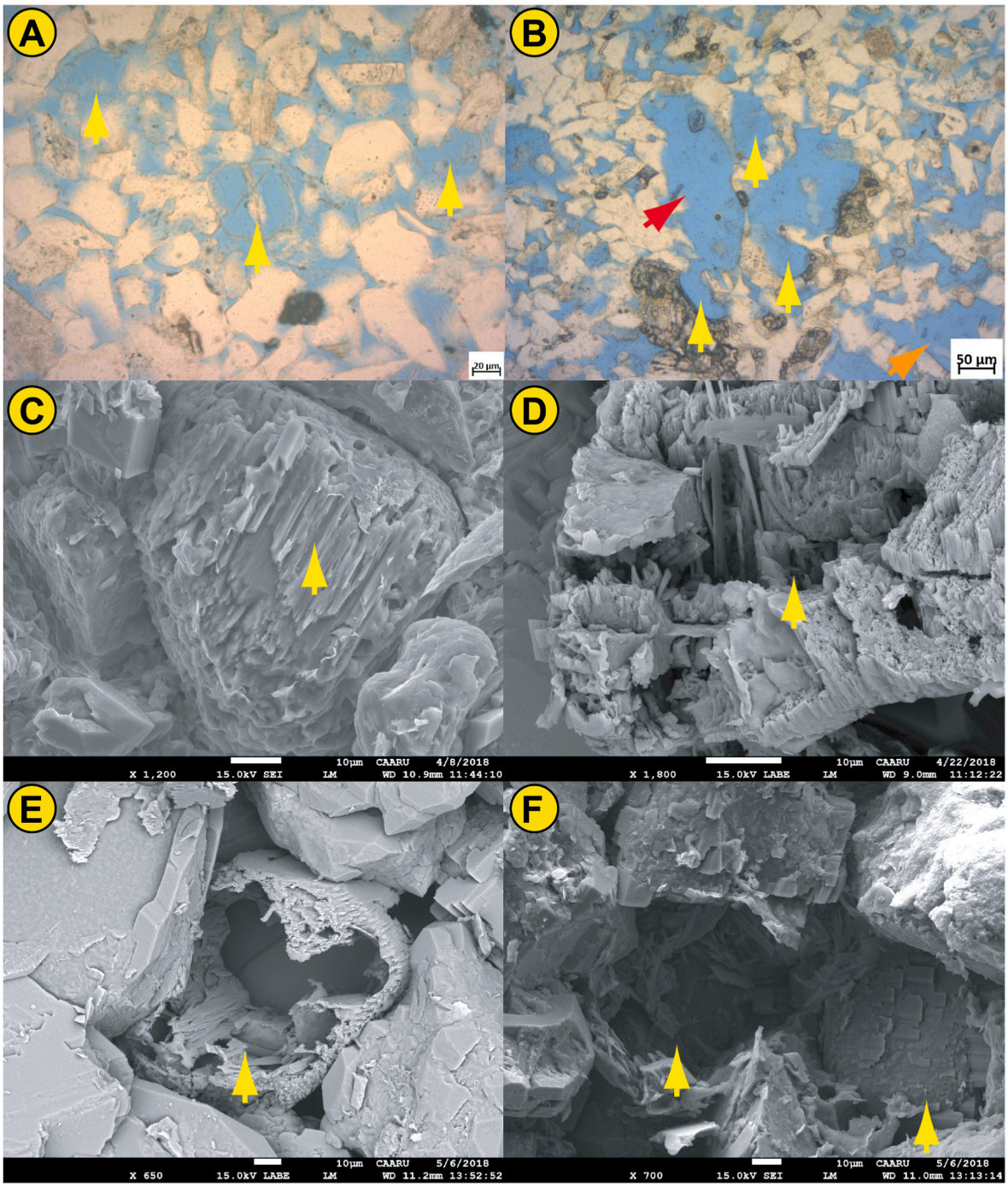

Fig. 18. Photomicrograph showing (A) dissolution of detrital feldspar grains with the remained feldspar skeletal (yellow arrows) (PPL), (B) dissolution of unknown grains (yellow grains), mudclast (red arrow), and matrix (orange arrow) (PPL), (C) SEM image showing leaching of feldspar grain (yellow arrow), (D) SEM image showing partial dissolution of feldspar grain (yellow arrow), (E) SEM image showing complete dissolution of feldspar grain (yellow arrow), and (F) SEM image showing two adjacent feldspar grains forming an oversized pore (yellow arrow).

or cementation (Fig. 19A). The micro-sized intergranular pores are more challenging to quantitatively assess but are mainly small remaining pores following compaction and cementation processes (Figs. 19B–E).

Secondary intragranular macro-sized pores result from matrix dissolution between grains (Fig. 19C). These macro-sized intragranular pores mainly arise from the partial dissolution of feldspars and micas (Figs. 19D–F). In contrast, moldic pores are associated with the complete dissolution of feldspar and mica grains (Figs. 19D–F). Secondary intercrystalline micro-sized pores are also challenging to quantitatively assess under the petrographic microscope but are mainly intercrystalline pores situated between clay crystals (i.e., predominantly kaolinite) and as intragranular micropores within albitized feldspars (Figs. 11E–19E).

While the modal composition analysis shows a wide range of total thin-section porosity ranging from 3% to 30.7%, there is no significant variation in the distribution of average total porosity among different facies associations within the fine-grained hybrid energy delta of the Barik Formation (Table 1; Fig. 20A). Nevertheless, the lowest minimum total porosity is observed within the mouth bar/shoreface and tidal channel facies associations (av. 4.7 vol% and 6.0 vol%, respectively), while the highest is found within the tidal flat and delta distributary

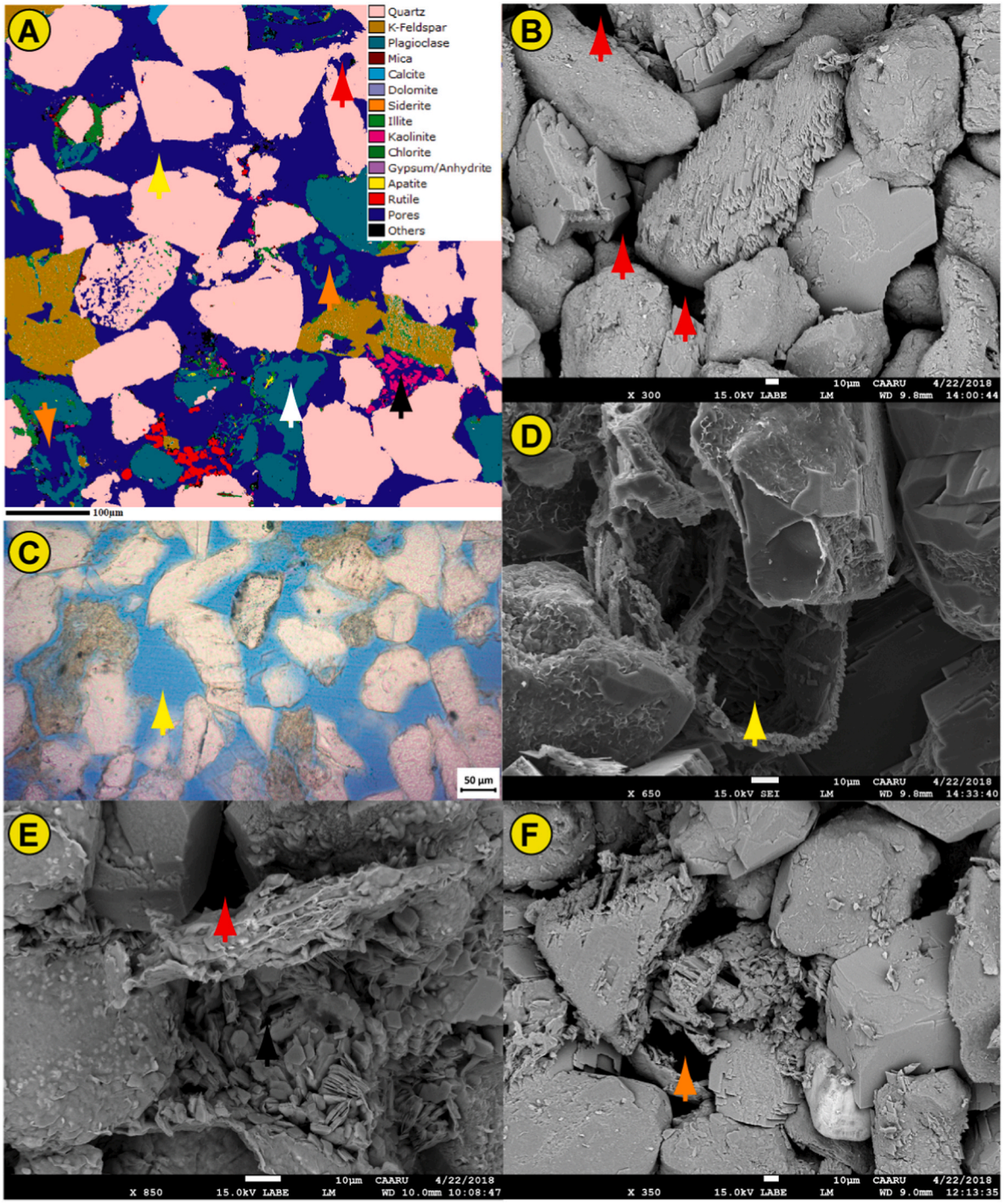

Fig. 19. QEMScan image showing macro-sized primary intergranular pores (yellow arrow), micro-sized primary intergranular pores (red arrow), macro-sized secondary intragranular pores (orange arrows), micro-sized secondary intragranular pore (white arrow), and micro-sized secondary intercrystalline pores (black arrow), (B) SEM image showing macro-sized primary intergranular pores (red arrows), (C) photomicrograph showing macro-sized secondary moldic pore (yellow arrow) (PPL), (D) SEM image showing macro-sized intragranular pore (yellow arrow), (E) SEM image showing micro-sized primary intergranular pore (red color) and micro-sized secondary intercrystalline pores (orange arrow), and (F) SEM image showing micro-sized secondary intragranular pore (orange arrow).

channel facies associations (av. 11.0 vol% and 12.3 vol%, respectively) (Fig. 20A).

A similar trend is observed for average thin-section primary porosity, ranging from 3% to 29.3%, with no noticeable variation among different facies associations (Table 1; Fig. 20B). The lowest minimum primary porosity is within the mouth bar/shoreface and tidal channel facies associations (av. 3.0 vol% and 3.7 vol%, respectively), and the highest is within the tidal flat and delta distributary channel facies associations (av. 10.3 vol% and 11.3 vol%, respectively).

While the contribution of secondary porosity to total porosity is not significant (av. 2.7 vol%), the highest secondary porosity is observed in the mouth bar/shoreface and tidal channel facies associations (av. 10.7 vol% and 11.7 vol%, respectively), and the lowest is within the tidal flat and delta distributary channel facies associations (av. 6.0 vol% and 7.7 vol%, respectively) (Table 1; Fig. 20C). The total intergranular volume versus total intergranular cement plot illustrates that primary porosity is

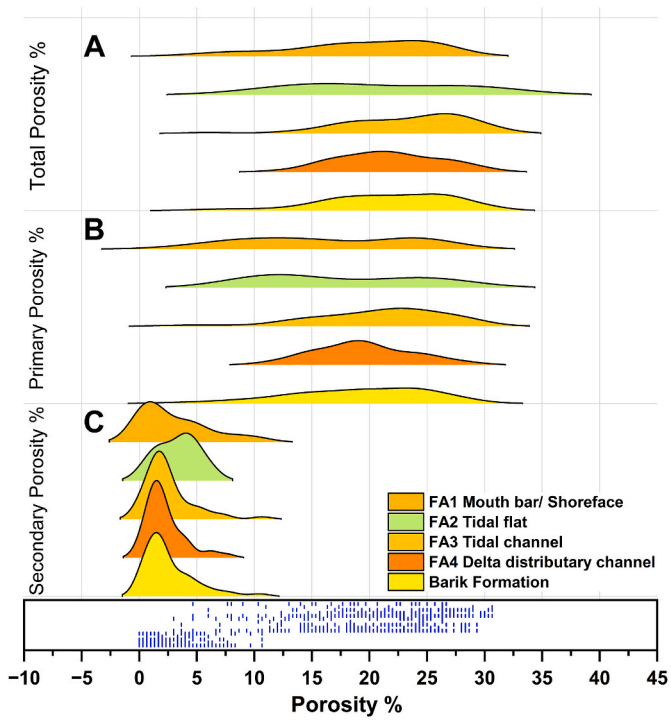

Fig. 20. Ridgeline chart showing (A) total porosity, (B) primary porosity, and (C) secondary porosity range of the Barik Formation and all facies associations.

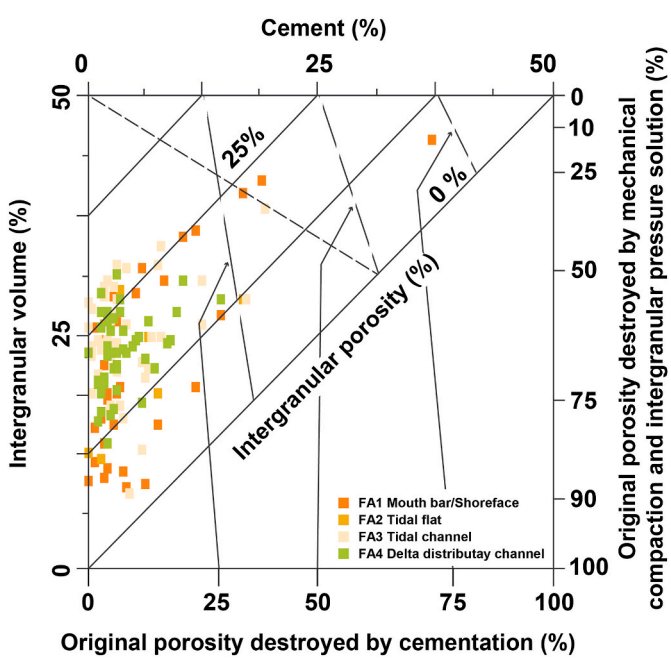

Fig. 21. Intergranular volume (IGV) vs intergranular cement (IGC) cross-plot (Houseknecht, 1988; modified by Ehrenberg, 1989) of all Barik Formation facies associations showing the effect of compaction on porosity reduction than cement.

predominantly modified by compaction, with a lesser influence from cementation (Fig. 21).

5. Discussion

5.1. Paragenetic sequence history

The paragenetic sequence history of the operated diagenetic processes affected the Barik Formation studied samples was assembled based on (i) textural relationship among the observed diagenetic alterations using the conventional microscope, SEM, and BSI examinations, (ii) character of intergranular pore-filling cement relative to the degree of compaction, and (iii) isotopic measurements of the carbonate cement. However, the precise timing and extent of each diagenetic process cannot be fully inferred, and thus a relative timing and duration are instead presented herein (Fig. 22).

The diagenetic history revealed the effect of climate conditions and surface waters during eodiagenesis followed by the effect of progressive burial conditions, i.e., pressure, temperature, and evolved formation waters chemistry during mesodiagenesis. Moreover, the effect of surface conditions after uplifting during telodiagenesis cannot be excluded. The eogenetic alterations are represented by the presence of mechanical infiltrated clays and iron-oxide coating grains, early dissolution and kaolinitization of feldspars, micas, and mud intraclasts, early dolomite and calcite, and silica cement, and mechanical compaction. The mesogenetic alterations, on the other hand, are represented by illitization and chloritization of mechanical infiltrated clays and kaolinite, chemical compaction, late dolomite and calcite cement, quartz overgrowth, and feldspar overgrowth, albitization of K-feldspar, late dissolution and kaolinitization of feldspars, and anhydrite cement. Thus, the presented herein diagenetic processes history and the products of the studied samples from the outcropped Barik Formation shares similarities with that of the studied and presented by Ramseyer et al. (2004) for the subsurface Barik Formation.

5.2. Eodiagenetic processes

5.2.1. Smectite

The light-yellow interference color nature of smectite with honeycomb texture covering the entire and along the contact between detrital grains (i.e., quartz and feldspar) surface suggests the formation by a mechanical infiltration process at the near-surface during eodiagenesis (Figs. 23A–C). Similar smectite nature and texture are reported by numerous researchers in the literature supporting the mechanical infiltration processes of the smectite origin (Wilson and Pittman, 1977;

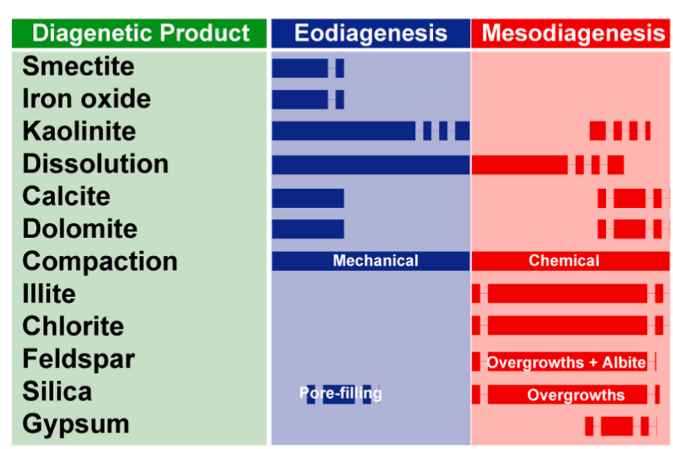

Fig. 22. Summary sketch showing the relative paragenetic sequence of the observed diagenetic alterations of the studied Barik Formation samples based on petrography and isotopes of carbonates.

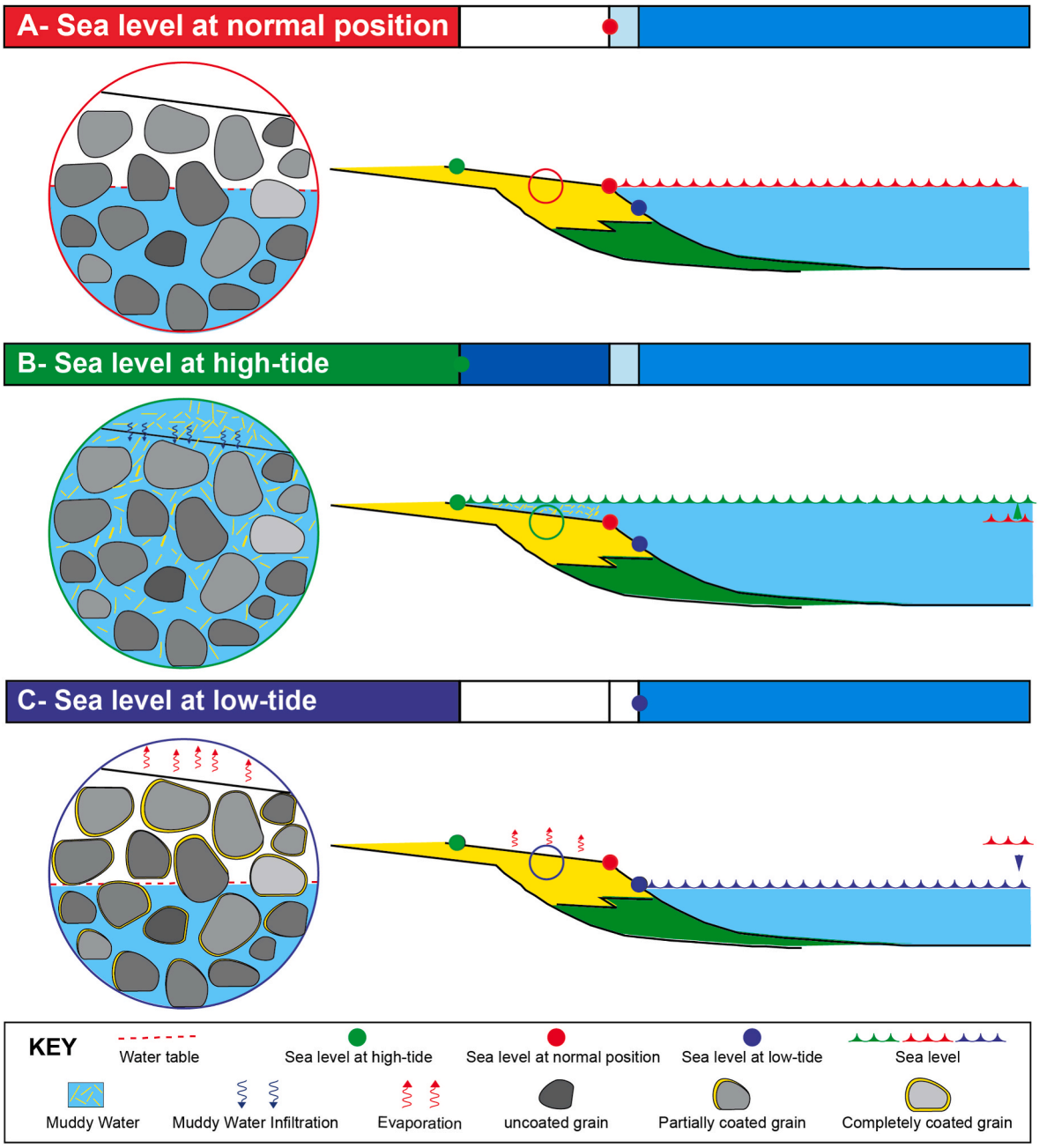

Fig. 23. Sketched cartoon summarizing the development of smectite clays by tidal pumps into the Barik Formation deposits. (a) Sea-level at normal position showing the subaerially exposed sediments landward areas in which the pore-waters between sediment grains above the water table are drain out, (b) a succeeding high-tide event pressurized the clayey waters to percolate into the already drained-out pores in between the sediment grains, and (c) the following low-tide event allowed the clayey waters to drain-out and clay fraction to settle down and coat the detrital grains.

Matlack and Hous, 1989; Moraes and De Ros, 1990, 1992; Critelli and Nilsen, 1996; El-Ghali et al., 2006a; Barbera et al., 2011; Caracciolo et al., 2014). Additionally, Ramseyer et al. (2004) reported the existence of smectite coating detrital grains in the subsurface Barik Formation sandstones and attributed that into the mechanical infiltration processes.

Accordingly, it is agreed that the formation processes of the smectite within the Barik Formation is attributed to the infiltration of clay fractions into the silts and sands through the percolation of the clayey-rich waters hydrodynamically by the tidal pumps force (Figs. 23A–C). The clayey-rich waters, prevalent during high tides, flow over and pressurized into the interconnected silt and sand pores (Fig. 23B). The subsequent subaerial exposure of the silt and sand during low tide cycles resulted in the drainage of the interconnected silt and sand pores and the remained clay fractions coats the grains (Fig. 23C). Thus, the repetition and intensity of high and low tide cycles increase the opportunity to develop the mechanically infiltrated smectite coating grains. The abundant smectite clays in the tidal channel siltstones and sandstones in comparison with the other facies association can be related to the intensity of tidal pumps within the tidal channels. The intense tidal pumps aid the clayey-rich waters to circulate into the siltstones and sandstones forming a fairly widespread smectite envelops around silt and sand grains. The relative thin smectite coats around the grains (i.e., 2–5 μm) in the tidal channel and mouth-bar/shoreface sandstones can be attributed to the nature of the fine to very fine sand grains (cf. Shelukhina, 2021).

It should be noted that the growth of mechanically infiltrated smectite coats around grains is related to the prevalent climate condition; being predominant in an arid to semi-arid condition (cf. Keller, 1970; Moraes and De Ros, 1992; El-Ghali et al., 2006a; Shelukhina et al., 2021a) and, to a less extent, a semi-humid condition (El-Ghali et al., 2006a). The prevalent semi-arid to semi-humid climate condition throughout the Upper Cambrian-Lower Ordovician (Al Kiyumi, 2019) are accountable for developing mechanically infiltrated clays in Barik

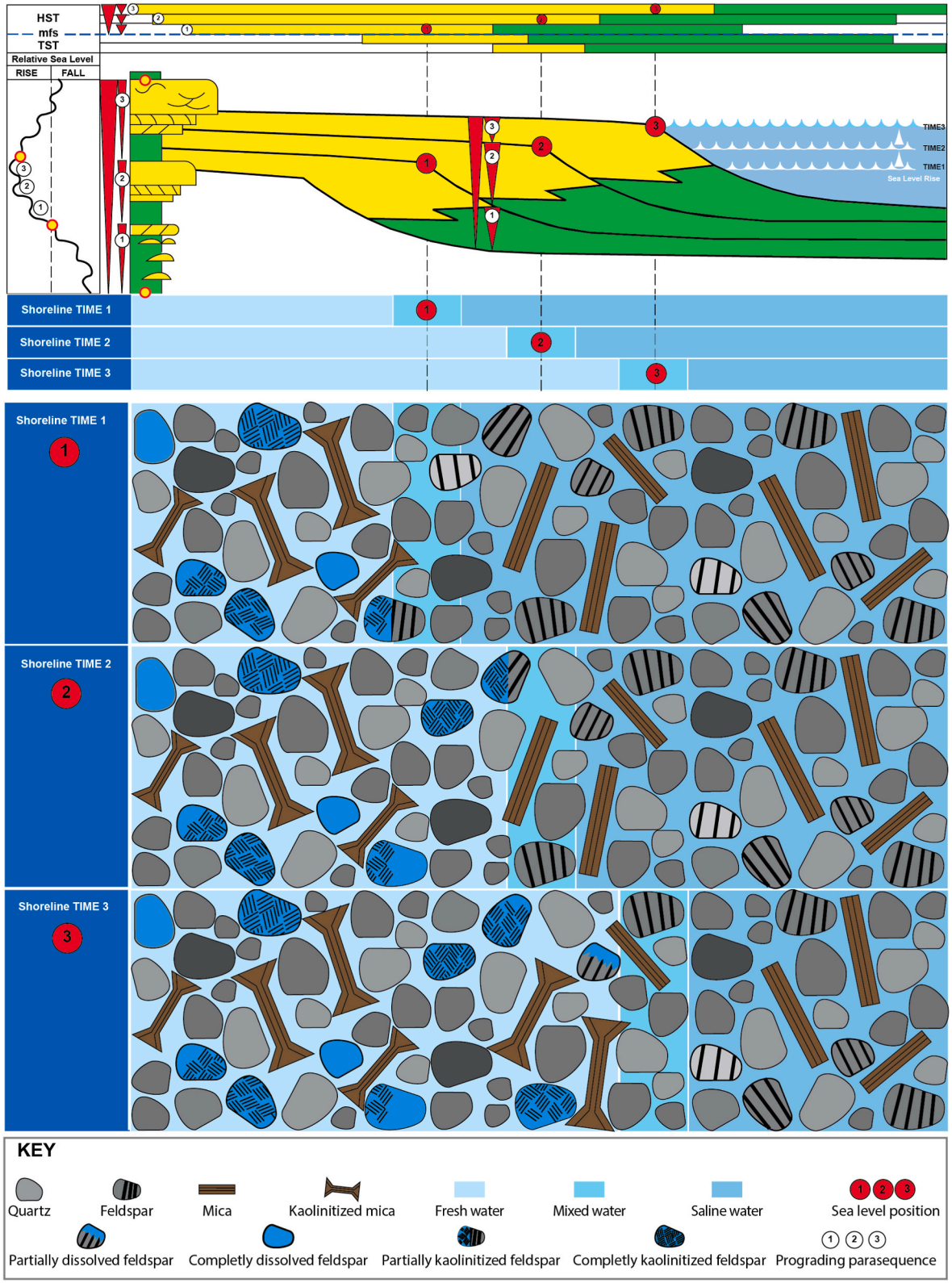

Fig. 24. Sketched cartoon summarizing the kaolinite formation via the interaction between the meteoric waters and chemically unstable silicate detrital grains such as feldspars and micas. Influx of meteoric waters into the sediments is enhanced by shoreline migration basinward areas (i.e. shoreline time 1 to shoreline time 3 through shoreline time 2).

Formation siltstones and sandstones.

5.2.2. Kaolinite

Kaolinite is a common diagenetic clay in sandstones and its formation is typically related to the dissolution of detrital silicate grains through (i) meteoric waters that invade the sandstones at the near-surface and shallow burial depths throughout eodiagenesis (cf. Meisler et al., 1984; Morad et al., 2000; El-Ghali et al., 2006a-b; El-Ghali et al., 2019), (ii) organic acids that are produced by the thermally maturated organic materials or that belong to CO_2 from nearby oil and coal shales at a deep burying depth during mesodiagenesis (Surdam et al., 1989; Hayes and Boles, 1992; Macaulay et al., 1993; Lanson et al., 1996; El-Ghali et al., 2006a-b), and (iii) meteoric waters invasion along and beneath the subaerial exposure surfaces during telodiagenesis (El-Ghali et al., 2006b). In the examined samples of Barik Formation, the occurrence of (i) kaolinite crystals in association with the expanded texture of micas, and (ii) kaolinite crystals in association with the non-compacted detrital feldspars, mud intraclasts, and filling nearby intergranular pores is evident that kaolinite has formed during eodiagenesis rather than meso- and/or telodiagenesis. The formation of kaolinite during eodiagenesis is related to the interaction of the micas, feldspars, and mud intraclasts with meteoric waters (Fig. 24). The meteoric waters circulation into the siltstones and sandstones to facilitate the interaction at near-surface and shallow burial depths was seemingly occurred owing to basinward shift of the shoreline during HST in concomitant with the deposition of Barik Formation (Fig. 24). The interaction to form kaolinite was greatly enhanced by multiple periods of semi-humid and to a less extent by semi-arid climatic conditions; this climatic condition was prevailed during the deposition of Barik Formation (Al-Kiyumi, 2019). Such kaolinite formation was reported in numerous siliciclastic sequences elsewhere (El-Ghali et al., 2006c; 2019).

5.2.3. Calcite

Calcite is a common eo-, meso-, and telodiagenetic alteration in siltstones and sandstones. Based on the petrographic data of the studied Barik Formation sandstones, the calcite cement filling large-sized intergranular pores support precompactional precipitation during eodiagenetic regime. The calcium ions required to accomplish the cementation by calcite are assumed to be sourced from the sea water. This assumption is supported by the fact that Barik Formation siltstones and sandstones lack Ca-rich constituents such as detrital carbonate grains and bioclasts. The bulk $\delta^{18}O_{VPDB}$‰ and $\delta^{13}C_{VPDB}$‰ values are believed to shed new insights on the source of the calcite cement. Using the bulk $\delta^{18}O_{VPDB}$ values from −9.05‰ to −5.54‰ of calcite cement filling uncompacted (i.e., loosely packed) framework grains (Table 2; Fig. 13), the fractionation equation of Friedman and O'Neil (1977), and anticipating that precipitation has occurred at near-surface and shallow depths with $\delta^{18}O_{SMOW}$ −8‰ to −6‰ of the Late Cambrian-Early Silurian Sea water (Veizer et al., 1999), suggest that cementation has precipitated at temperatures between 20 and 55 °C. These temperatures are compatible with the pre-compactional calcite that forms during eo-diagenetic realm. Moreover, the high $\delta^{13}C_{VPDB}$ values (−4.36‰ to −2.26‰) of calcite cement suggest that carbon was marginally depleted relative to the Cambrian-Ordovician marine values (−0.1‰ to −3.2‰; Veizer et al., 1999) through the input from inorganic source derived from continental waters. The scarcity of calcite cement in the studied Barik Formation siltstones and sandstones is attributed to (i) the lack of detrital carbonate grains and bioclasts; the source of the required ions for calcite cement and (ii) high rate of sedimentation (i.e. short residence time); it is known than carbonate cement precipitation is facilitated by the prolonged residence time of sediments in close proximity to the sea floor and at shallow depths, which occurs due to low sedimentation rates allowing the sediments to remain at a consistent and optimal geochemical conditions.

5.2.4. Dolomite

Dolomite is a common eo-, meso-, and telodiagenetic alteration in sandstones. Based on the petrographic data of the studied Barik Formation sandstones showing the dolomite cement filling large-sized intergranular pores support precompactional precipitation during eodiagenetic regime. The calcium and magnesium ions required to accomplish the cementation by dolomite are assumed to be sourced from the sea water. This assumption is supported by the fact that Barik Formation sandstones lack Ca- and Mg-rich constituents such as detrital carbonate grains and bioclasts. However, the $\delta^{18}O_{VPDB}$‰ and $\delta^{13}C_{VPDB}$‰ values helped to shed new insights on the source of the dolomite cement. Using the bulk $\delta^{18}O_{VPDB}$ values from −8.63‰ to −5.95‰ of dolomite cement (Table 2; Fig. 13), the fractionation equation of Friedman and O'Neil (1977), and anticipating that precipitation has occurred at near-surface and shallow depths with $\delta^{18}O_{SMOW}$ −8‰ to −6‰ of the Late Cambrian-Early Silurian (Veizer et al., 1999), suggest that cementation has occurred at temperatures between 40 and 75 °C. These temperatures are compatible with the eodiagenetic regime and subsequent progressive burial. The high $\delta^{13}C_{VPDB}$ values −4.37‰ to −1.87‰ of the sandstone samples dominated by dolomite cement suggest that carbon was marginally depleted relative to the Cambrian-Ordovician marine values (−3.2‰ to −0.1‰; Veizer et al., 1999) through the input from inorganic sources derived from continental waters. The scarcity of dolomite cement in the studied Barik Formation sandstones is attributed to (i) the lack of detrital carbonate grains and bioclasts; the source of the required ions for dolomite cement and/or (ii) high rate of sedimentation (i.e. short residence time); it is known than carbonate cement growth is facilitated by the prolonged residence time of sediments in close proximity to the sea floor and at shallow depths, which occurs due to low sedimentation rates allowing the sediments to remain at a consistent and optimal geochemical conditions.

5.2.5. Mechanical compaction

Mechanical compaction in sandstones is a common eodiagenetic phenomenon. It is well-known that the extent of mechanical compaction is governed by the sedimentation rate and early cementation; the greater the sedimentation rate and a lesser amount of early cementation, the greater degree of compaction and vice versa. However, in most of the studied Barik Formation siltstones and sandstones, mechanical compaction is widespread due to the scarcity of eodiagenetic intergranular cement. In addition to the scarcity of eodiagenetic intergranular cement, mechanical compaction is more intense in sandstones containing abundant micas. The intense mechanical compaction in sandstones lacking eodiagenetic intergranular cement and containing abundant micas (i.e. physically unstable) is attributed to high sedimentation rates prevailed during the deposition of HST of Barik Formation. Contrariwise, a lesser degree of mechanical compaction is noticed in some of the mouthbar/shoreface where the eodiagenetic calcite and dolomite cements have found.

5.3. Mesodiagenetic processes

5.3.1. Kaolinite

In the studied Barik Formation sandstones, the occurrence of (i) kaolinite postdating quartz overgrowths, (ii) a concave-convex intergranular contact of the outline of the kaolinitized feldspar, and (iii) illitized some of the kaolinite crystals, support the formation during mesodiagenesis rather than telodiagenesis. The exclusion of telodiagenetic origin of kaolinite is supported by the fact that this kaolinite has undergone illitization; which is the process that predominates during deep burial depth (i.e., mesodiagenesis). The mesodiagenetic kaolinite was achieved by the dissolution of unstable detrital feldspar grains via acidic fluids. The acidic fluid in deep burial (mesodiagenesis regime) is usually attributed to the organic acids (Surdam et al., 1984; Van Keer et al., 1998; El-Ghali et al., 2006b) or CO_2 from adjacent oil or coaly

shales. The CO2 can also be produced inorganically. However, the acidic fluid in the studied Barik Formation sandstones is difficult to establish because the mudstones of Barik Formation lack organic material and thus lack the production of organic acids.

5.3.2. Illite

The yellow color of the tangentially projected illitic grain-coating clays around detrital grains (i.e. quartz and feldspar) surface and at the contact between grains as described and confirmed by the optical microscope, XRD, SEM, and EDS investigations suggest an authigenic origin for these clays formation. Moreover, the conserved honeycombs and cornflakes texture along with their filamentous terminations of the illite in Barik Formation sandstones support the transformation from the mechanically infiltrated smectite during mesodiagenesis (El-Ghali et al., 2006a; Shelukhina et al., 2021a). It is reported by several researchers that the mesodiagenetic origin of illite is typically characterized by honeycombs, cornflakes, fibrous, mat-like, and lath-like morphology texture with filamentous and spiny termination (Worden and Morad, 2000; El-Ghali et al., 2006a). The transformation of smectite into illite typically takes place via the mixed-layer smectite-illite. Yet, such a mixed layer is not identified in the studied samples. However, the presence of fibrous and lath-like texture at the kaolinite edges supports the transformation of kaolinite into illite (cf. Morad et al., 2000; El-Ghali et al., 2006b). It is well-known that the illitization process, i.e., illitization of smectite and kaolinite, may start at ca. 70 °C and is prevalent at temperatures higher than ca. 130 °C (Ehrenberg and Nadeau, 1989; Morad et al., 2000; Giles et al., 1992; Worden and Morad, 2000). The accomplishment of the illitization process needs the presence of potassium ions in the pore-water (i.e., a high aK^+/aH^+ ratio; Morad et al., 2000; S Morad et al., 2010; Al-Ramadan, 2014; El-Ghali et al., 2019). The needed potassium ions to elevate the aK^+/aH^+ ratio to complete the illitization process in the studied samples are seemingly obtained internally (closed-system diagenesis) thru the dissolution of potassium-type feldspars. However, externally sourced (open-system diagenesis) potassium ions from alkali metals (Furlan et al., 1996; Land et al., 1997) cannot be excluded. So, the abundance of illite is seemingly associated with the availability of potassium ions in pore.

5.3.3. Chlorite

The grayish- and pale green-colored XPL and PPL; respectively of platelet-like morphology texture of chlorite coating around and at the contact between detrital grains (i.e., quartz and feldspar) as described and confirmed by the optical microscope, XRD, SEM, and EDS investigations suggest an authigenic origin for these clays' formation. The platelet-like texture of chlorite with a perpendicular arrangement on grains surface and along grain-to-grain contact is indicative for precursor clays conversion into chlorite during mesodiagenesis (Shelukhina et al., 2021a). The conversion of precursor clays into chlorite is well-documented in the literature by several researchers (Moraes and De Ros, 1992; Humphreys et al., 1994; Ryu and Niem, 1999; Anjos et al., 2003; Worden and Morad, 2003). Odinite, berthierine, and smectitic clays are common precursor clays for chlorite formation (Jahren and Aagaard, 1989; Odin, 1990; Ehrenberg, 1993; Humphreys et al., 1994; Morad et al., 2000; S. Morad et al., 2010; Beaufort et al., 2015; Saïag et al., 2016; Al-Ramadan et al., 2017; Worden et al., 2020). The precursor clays for chlorite in the studied samples are apparently the mechanically infiltrated magnesian smectite, as proved by the EDS examination (i.e., Mg-rich chlorite). The chloritization of the precursor Mg-smectite clays is common during mesodiagenesis realm with the availability of iron ions. The availability of iron ions to accomplish the chloritization in these sandstones is seemingly obtained internally (closed-system diagenesis) thru the grain-coating iron-oxides. The scantiness of chlorite compared with illite clays is apparently attributed to the insufficiency of iron ions in pore waters.

5.3.4. Chemical compaction

Chemical compaction is a common mesodiagenetic phenomenon in sandstones. The intensity of chemical compaction is attributed to the shortage of early cementation; the lesser early cementation, the higher degree of chemical compaction, and vice versa are applicable. In most of the studied Barik Formation sandstones, the shortage of early intergranular cement accounted for the high intensity of chemical compaction. However, the cementation by quartz and feldspar overgrowths during progressive burial help to some extent the prevention of further compaction. The quartz and feldspar overgrowths crystals worked as grains support and thus stopped the compaction. Less degree of chemical compaction is noticed in some of the mouth-bar/shoreface sandstones where the early calcite and dolomite have prevailed.

5.3.5. Quartz overgrowths

Quartz overgrowths formation is typical in the mesodiagenesis relam (cf. Worden and Morad, 2000; El-Ghali et al., 2006a; Critelli et al., 2008, 2018). The amounts of quartz overgrowths in Barik Formation sandstones are governed mostly by eodiagenetic mechanically infiltrated and mesodiagenetic illite and chlorite coating grains, and chemical compaction. However, illite and chlorite coating grains are well-known to hinder cementation by quartz overgrowths (Ehrenberg, 1993; Morad et al., 2000; Shelukhina et al., 2021a). The source of the required silica for quartz overgrowths formation is evidenced by the existence of multiple diagenetic processes including pressure dissolution of detrital quartz grains, kaolinitization and albitization of K-feldspars, and illitization and chloritization of mechanically infiltrated clays. It is documented in the literature that such diagenetic processes are accounted as an internal source of silica (McBride, 1989; Worden and Morad, 2000). The postdating of quartz overgrowths, the illitization, and chloritization of the mechanically infiltrated clays indicates its precipitation during deep burial depth at high temperature (i.e., mesodiagenesis; 90–130 °C; McBride, 1989; Giles et al., 1992; Gluyas et al., 1993; Hartmann et al., 2000; Morad et al., 2000). The inferred deeply-buried origin of the quartz overgrowths at such elevated temperature in outcropped Barik Formation sandstones is in agreement with the calculated temperature (117–158 °C) that was reported by Ramseyer et al. (2004) for the subsurface Barik Formation sandstones.

5.3.6. Feldspar overgrowths

The precipitation of feldspar overgrowths may occur during the eo- and mesodiagenetic regimes (Morad et al., 2000; Critelli et al., 2008; El-Ghali et al., 2009). The postdating of feldspar overgrowths, the illitization, and the chloritization of the mechanically infiltrated clays indicate feldspar overgrowths precipitation has occurred during deep burial depth at high temperatures. The amounts of feldspar overgrowth in Barik Formation sandstones are controlled mostly by eodiagenetic alterations of mechanically infiltrated smectite and mesodiagenetic clays; illite and chlorite coating grains. However, illite and chlorite coating grains are known to hinder cementation by feldspar overgrowths (Shelukhina et al., 2021a). The high aSi and high aK+/aH + are required to precipitate K-feldspar overgrowths (Morad et al., 2000; El-Ghali et al., 2009). In the studied sandstones, the high aSi and high aK+/aH + have seemingly derived from the dissolution of unstable silicate grains, particularly feldspars and kaolinitization of k-feldspars during the mesodiagenetic relam.

5.3.7. Albitized feldspar

The albitization of feldspars may start at a relatively low temperature ca. 50 °C (Wopfner et al., 1991; Remy, 1994) and dominates at higher temperatures ≥130 °C (Bjørlykke and Brendsdal, 1986). Empirically, it is documented that the albitization process is temperature and heating rate dependent more than it is time and fluid chemistry (Perez and Boles, 2005); however, the source of sodium is still essential to accomplish the albitization process (Boles, 1982). The required sodium ions for the albitization process in the studied Barik Formation sandstones reflect the

availability of sodium in porewaters, which was seemingly derived later throughout the diagenetic reactions such as the illitization of the smectite (i.e., mechanically infiltrated clays). Illitization of mechanically infiltrated smectitic clays is predominant in the studied Barik Formation sandstones. The illitization of smectite is well-known to associate with the release of sodium ions (Boles and Franks, 1979).

5.3.8. Gypsum

Gypsum cement in sandstones commonly precipitates during the eo- and mesodiagenetic regime. The gypsum cement in the studied sandstones of the Barik Formation is interpreted to be of mesogenetic origin, as evidenced by its engulfment of quartz overgrowths and filling of small intergranular pores. The gypsum requires a source of calcium ions and sulfate to precipitate. Sulfate can be sourced internally; however, sulfate-bearing detrital grains are absent, and thus the internally sourced sulfate can be ruled out. Moreover, seawater cannot be considered the source of the required sulfates in the studied Barik Formation sandstones because the sulfate concentration depletes with progressive burial at greater depth, and accordingly, gypsum precipitation at greater depth where the deep flux of sulfate from seawater is impossible. Thus, the source of sulfates is challenging to establish; however, an external source is still the most favorable, and it is postulated to be a migrating fluid from the underlying Ara Salt rocks. Nevertheless, this postulated source of sulfates needs to be justified; however, the available data does not justify this postulated source. The required Ca ions to precipitate the gypsum can be sourced internally via the illitization of smectitic clays (i.e., mechanically infiltrated clays) and the kaolinitization of plagioclase processes.

5.3.9. Calcite

The origin of calcite cement that fills small-sized pores and post-dating quartz overgrowths remains enigmatic due to the absence of $\delta^{18}O_{VPDB}$ and $\delta^{13}C_{VPDB}$ data. However, the observed petrographic data may shed insights on its origin. The engulfment of quartz overgrowths by calcite suggests that calcite precipitation has occurred (i) during deep burial (i.e. mesodiagenesis) subsequent to quartz overgrowths, which are typically of mesogenetic origin (McBride, 1989; Worden and Morad, 2000) and/or subsequent to uplifting (i.e. telodiagenesis). However, due to the lack of isotopic data and the origin of calcite cement was not stated in Ramseyer et al. (2004) study for the subsurface Barik Formation siltstones and sandstones, the origin of calcite remains enigmatic.

5.3.10. Dolomite

The origin of dolomite cement that fills small-sized pores and post-dating quartz overgrowths remains engamtic due to the absence of $\delta^{18}O_{VPDB}$ and $\delta^{13}C_{VPDB}$ data. However, the observed petrographic data may shed insights on its origin. The engulfiment of quartz overgrowths by dolomite suggests that dolomite precipitation has occurred (i) during deep burial (i.e. mesodiagenesis) subsequent to quartz overgrowths, which are typically of mesogenetic origin (McBride, 1989; Worden and Morad, 2000) and/or (ii) subsequent to uplifting (i.e. telodiagenesis). The proposed mesogenetic origin for this type of dolomite cement is in line with that reported by Ramseyer et al. (2004) for the subsurface Barik Formation siltstones and sandstones. They concluded that the temperature at which this dolomite cement has precipitated ranges between 125 and 142 °C.

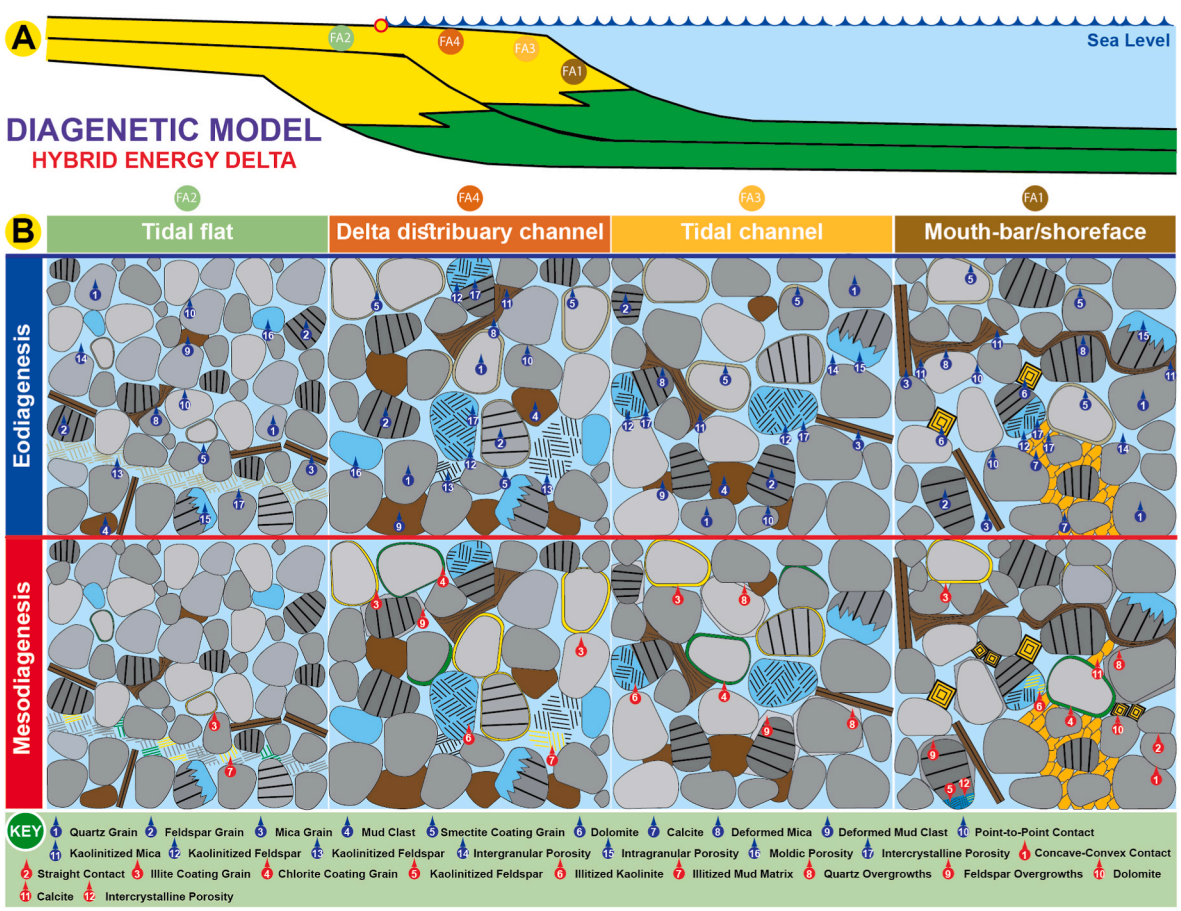

Fig. 25. Sketched cartoon summarizing the observed diagenetic alterations of the hybrid-energy delta system (A) amongst all facies associations of the Barik Formation during eo- and mesodiagenesis realms (B).

5.4. Diagenetic alterations and reservoir porosity evolution and distribution model

The Barik Formation hybrid-energy delta system siltstones and sandstones were deposited during a prograding highstand systems tract period (Shelukhina et al., 2021b). In such a depositional system of a prograding highstand system tract, marine and fluvial processes, high sedimentation rate, and alternating between marine and meteoric waters in addition to climate condition govern the types, extent, and distribution of eodiagenetic alterations and subsequently mesodiagenetic alterations (Fig. 25). Shortly after the time of deposition; at near surface and during high tides, clayey waters were pressured into the siltstones and sandstones by the tidal pumps and the subsequent low tides resulted in water draining and clay (i.e., smectite) formation (Shelukhina et al., 2021a). This clay is slightly effected porosity by blocking pores and narrowing pore throats at near surface during eodiagenesis, however, on the other hand it preserves porosity during deep burial (i.e., mesodiagenesis) by preventing the formation of quartz and feldspar overgrowths. The prograding of delta during the highstand system tract usually associates with basinward migration of meteoric waters and, thus, large areas were exposed to meteoric waters. These meteoric waters interacted and resulted in partial and complete dissolution of silicate grains including micas and feldspars and matrix and formation of kaolinite, leading to the development of micro- and macro-size secondary intragranular pores and moldic porosity during eodiagenesis. The development of mechanically infiltrated clays (i.e., smectite) and kaolinite is thought to be promoted by the prevalence of a semi-arid to semi-humid climatic conditions. The prograding delta coupled with high rate of sedimentation and the short residence time for the sediment in contact with sea waters led to the precipitation of small amounts of carbonate (i.e., calcite and dolomite) cement. The precipitation of small amounts of carbonate cement was enhanced by the absence of detrital carbonate grains and bioclasts, the source of needed Ca and Mg ions. Carbonate cement resulted in slight reduction of porosity during eodiagenesis specially in the mouth bar/shoreface siltstone and sandstones. Scarcity of early cementation facilitated the mechanical compaction, which is another predominant eodiagenetic process resulted in closely packed grains and pending micas and thus porosity reduction. During eaodiagenesis, compaction was more significant in reservoir porosity deterioration than cementation; however, dissolution played the main role in reservoir quality enhancement instead.

Mesodiagenetic alterations are further governed by the types and distribution of eodiagenetic alterations. During the mesodiagenesis realm, which is characterized by elevated temperatures, the smectite clays (i.e., mechanical infiltrated clays) in the presence of potassium and iron resulted in the formation of illite and chlorite, respectively. The domination of illite in comparison of chlorite is attributed to the availability of potassium ions than iron. Grain coating clays (i.e. smectite, illite, and chlorite), especially that riming the entire grains surface, hindered the formation of quartz and feldspar overgrowths and thus preserving reservoir porosity at greater depths. Moreover, the development of small quantities of quartz and feldspar overgrowths worked as a support for detrital grains from further compaction and thus preserving reservoir porosity. Other diagenetic alterations that are prevalent during mesodiagenesis but have no linkage to sequence stratigraphy include Illitization of kaolinite. Illitization is seemingly controlled by the availability of potassium ions that was, at least partially, sourced internally via the dissolution and albitization of potassium feldspar grains. Moreover, cementation by small amounts of calcite, dolomite, and gypsum has prevailed at later stage of the mesodiagenesis realm and resulted in slight reduction of reservoir porosity at greater depths.

6. Conclusions

This study investigated the outcrops of the highstand systems tract (HST) hybrid energy delta of the Upper Cambrian-Lower Ordovician Barik Formation in the Haushi-Huqf region of Central Oman using an integrated petrographic-depositional-sequence stratigraphic approach. The furthermost important findings of this study include.

- The Barik Formation is predominantly coarse-grained siltstones to fine-grained sandstones, moderately to very well-sorted, and arkosic- to subarkosic-arenites in composition.
- The sandstones underwent various degrees of diagenetic processes including compaction, dissolution, and cementation during the eo- and mesodiagenesis realms that have led to a mildly heterogeneous distribution amongst depositional facies and parasequences.
- Mechanical infiltrated clays (i.e., smectite) is a common diagenetic mineral that was developed at the near surface during eodiagenesis. It was developed as a result of the clayey waters percolation into the siltstones and sandstones hydrodynamically by tidal pumps. These clays have slightly affected the reservoir porosity during eodiagenesis; however, they positively preserve reservoir porosity during deep burial (i.e., mesodiagenesis) by hindering the cementation by quartz and feldspar overgrowths.
- Kaolitization of feldspar and mica grains is another common eodiagenetic mineral that was formed as a result of meteoric waters invasion into the siltstones and sandstones during basinward migration of the shoreline as the delta prograde during the highstand system tract.
- Calcite and dolomite with small quantities are another eodiagenetic minerals. Their small quantities are related to the lack of detrital carbonate grains and bioclasts (the provider of Ca and Mg needed for cementation) and high rate of sedimentation (i.e., short residence time) enhanced by delta prograding during HST. The shortage of eodiagenetic cement led to mechanical compaction, resulting in a reduction in reservoir porosity.
- Formation of illite and chlorite as mesodiagenetic minerals via illitization and chloritization of the mechanically infiltrated clays (i.e., smectitic) that was facilitated by the elevated temperature and the availability of potassium and iron ions. The ions were sourced internally through the dissolution of potassium feldspars and formation of kaolinite and albitization of potassium feldspars.
- Overgrowths of quartz and feldspar, serving as mesodiagenetic minerals on clean and/or discontinuously coated grains with smectite, illite, and chlorite. These quartz and feldspar overgrowths resulting in porosity reduction; however, they supported the detrital grains from further compaction and thus may limit further porosity reduction.
- Intense feldspar dissolution and kaolinitization during mesodiagenesis have been positively enhanced reservoir quality.
- Formation of small quantities of calcite, dolomite, and gypsum mesodiagenetic minerals at the later stage of mesodiagenesis realm filling the remained intergranular pores leading to an insignificant reduction of reservoir porosity.

This study demonstrated that the shortage of early cementation and instead the occurrence of intense compaction have played a role in reservoir porosity deterioration. On the other hand, the developement of of mechanically infiltrated clays in the siltstones and sandstones during eodiagenesis helped in preserving the reservoir porosity by hindering the development of quartz and feldspar overgrowths during mesodiagenesis.

Declaration of competing interest

The authors declare that they have no known competing financial interests or personal relationships that could have appeared to influence the work reported in this paper.

Data availability

Data will be made available on request.

Acknowledgments

This research work is financed by His Majesty's Strategic Fund [SR/SCI/ETHS/15/01] to Sultan Qaboos University. Abdalla Al Fahdi, Hamdan Al-Zidi, Bader Al Waili, Bader Al Shaqsi, Said Al-Abri, and Hilal Al-Zidi at the Department of Earth Sciences, Sultan Qaboos University, are acknowledged for their logistical, software, and microscope-related support. Ruslan Abylopsis, Junaid Khan, and Yasin Alizade are acknowledged for their support and assistance in the field. The Central Analytical and Applied Research Unit (CAARU) laboratories at Sultan Qaboos University, Sultanate of Oman, are acknowledged for the support with XRD, SEM, EDS analysis. The Center for Integrative Petroleum Research at King Fahd University of Petroleum and Minerals, Dhahran, Saudi Arabia, is acknowledged for the support with QEMSCAN analysis.

References

Al Kiyumi, A.K.M., 2019. Provenance, Petrofacies and Paleoclimate of Al Bashair and Barik Formations, Al-Huqf Area, Central Oman. Unpublished MSc. thesis, Sultan Qaboos University, p. 166.

Al Marjibi, S., 2011. Unravelling the Depositional Environments within the Lower Andam Group of North-Central Oman. Ph.D. thesis, University of Aberdeen, Scotland, p. 366.

Al-Ramadan, K., Morad, S., Proust, J.N., Al-Aasm, I.S., 2005. Distribution of diagenetic alterations within the sequence stratigraphic framework of shoreface siliciclastic deposits: evidence from Jurassic deposits of NE France. J. Sediment. Res. 75, 943–959.

Al-Ramadan, K., 2014. Illitization of smectite in sandstones: the permian unayzah reservoir, Saudi Arabia. Arabian J. Sci. Eng. 39 (1), 407–412.

Al-Ramadan, K., Franks, S.G., Al-Shammari, S., Rees, A., Koeshidayatullah, A., Abu-Khamsin, S., 2017. Depositional and diagenetic barriers, baffles and conduits: permian–Carboniferous Unayzah reservoir, Nuayyim field, Central Saudi Arabia. J. Petrol. Geol. 40 (1), 85–103.

Amendola, U., Perri, F., Critelli, S., Monaco, P., Cirilli, S., Trecci, T., Rettori, R., 2016. Composition and provenance of the macigno formation (late oligocene-early miocene) in the trasimeno lake area (northern apennines). Mar. Petrol. Geol. 69, 146–167. https://doi.org/10.1016/j.marpetgeo.2015.10.019.

Anjos, S.M.C., De Ros, L.F., Silva, C.M.A., 2003. Chlorite authigenesis and porosity preservation in the Upper Cretaceous marine sandstones of the Santos Basin, offshore eastern Brazil. In: Worden, R., Morad, S. (Eds.), Clay Mineral Cements in Sandstones, vol. 34. Int. Assoc. Sedimentol. Spec. Publ, pp. 283–308.

Bailey, E.H., Stevens, R.E., 1960. Selective staining of K-feldspar and plagioclase on rock slabs and thin secti·ons. American Mz;neYtllogist 45, 1020–1025.

Barbera, G., Critelli, S., Mazzoleni, P., 2011. Petrology and geochemistry of Cretaceous sedimentary rocks of the Monte Soro Unit (Sicily, Italy): constraints on weathering, diagenesis and provenance. J. Geol. 119, 51–68. https://doi.org/10.1086/657340.

Beaufort, D., Rigault, C., Billon, S., Billault, V., Inoue, A., Inoué, S., Ferrage, E., 2015. Chlorite and chloritization processes through mixed-layer mineral series in low-temperature geological systems–a review. Clay Miner. 50 (4), 497–523.

Bhattacharya, J.P., Giosan, L., 2003. Wave-influenced deltas: geomorphological implications for facies reconstruction. Sedimentology 50, 187–210.

Bhattacharya, J.P., Walker, R.G., 1992. Deltas. In: Walker, R.G., James, N.P. (Eds.), Facies Models: Response to Sea Level Change. Geological Association of Canada, St Johns, NF, pp. 157–177.

Bjørlykke, K., Brendsdal, A., 1986. Diagenesis of the Brent Sandstone in the Statfjord Field. North Sea.

Boles, J.R., 1982. Active albitization of plagioclase, gulf coast Tertiary. Am. J. Sci. 282 (2), 165–180.

Boles, J.R., Franks, S.G., 1979. Clay diagenesis in the Wilcox sandstones of southern Texas: implications of smectite diagenesis on sandstone cementation. J. Sediment. Petrol. 49, 55–70.

Buckley, R.C., 1997. The Sedimentary Evolution of the Cambrian of East-Central Oman: an Outcrop Study of the Haima Supergroup. Unpublished PhD thesis, University of London (Birbeck College and University College), p. 331.

Caracciolo, L., Arribas, J., Ingersoll, R.V., Critelli, S., 2014. The diagenetic destruction of porosity in plutoniclastic petrofacies: the Miocene Diligencia and Eocene Maniobra formations, Orocopia Mountains, southern California, USA. In: Scott, R.A., Smyth, H. R., Morton, A.C., Richardson, N. (Eds.), Sediment Provenance Studies in Hydrocarbon Exploration and Production, vol. 386. Geological Society, London, Special Publication, pp. 49–62. https://doi.org/10.1144/SP386.9.

Cocks, L.R.M., Torsvik, T.H., 2002. Earth Geography from 500 to 400 Million Years Ago: A Faunal and Palaeomagnetic Review, vol. 159. Journal of the Geological Society, London, pp. 631–644.

Civitelli, M., Ravidà, D.C.G., Borrelli, M., Criniti, S., Falsetta, E., 2023. Diagenesis and petrophysics of miocene sandstones within southern apennines foreland. Italy: Mar. Petrol. Geol. 155, 1–16. https://doi.org/10.1016/j.marpetgeo.2023.106411, 106411.

Coleman, J.M., 1981. Deltas: Processes of Deposition and Models for Exploration. Burgess Publishing Co., Minneapolis, MN.

Coleman, J.M., Roberts, H.H., 1989. Deltaic coastal wetlands. Geol. Mijnbouw 68, 1–24.

Coleman, J.M., Roberts, H.H., Stone, G.W., 1998. Mississippi River delta: an overview. J. Coast Res. 14, 698–716.

Corrado, S., Aldega, L., Perri, F., Critelli, S., Muto, F., Schito, A., Tripodi, V., 2019. Detecting syn-orogenic and sediment provenance of the Cilento wedge top basin (southern Apennines, Italy) by mineralogy and geochemistry of fine grained sediments and petrography of dispersed organic matter. Tectonophysics 750, 404–418. https://doi.org/10.1016/j.tecto.2018.10.027.

Courjault-Rade, P., Debrenne, F., Gandin, A., 1992. Palaeogeographic and geodynamic evolution of the Gondwana continental margins during the Cambrian. Terra. Nova 4, 657–667.

Critelli, S., Nilsen, T.H., 1996. Petrology and diagenesis of the eocene butano sandstone, LaHonda basin, California. J. Geol. 104, 295–315. https://doi.org/10.1086/629826.

Critelli, S., Mongelli, G., Perri, F., Martin-Algarra, A., Martín-Martín, M., Perrone, V., Dominici, R., Sonnino, M., Zaghloul, M.N., 2008. Sedimentary evolution of the middle triassic -lower jurassic continental redbeds from western-central mediterranean alpine chains based on geochemical, mineralogical and petrographical tools. J. Geol. 116, 375–386. https://doi.org/10.1086/588833.

Critelli, S., Perri, F., Arribas, J., Herrero, M.J., 2018. Sandstone detrital modes and diagenetic evolution of Mesozoic continental redbeds from western-central circum-Mediterranean orogenic belts. In: Ingersoll, R.V., Lawton, T.F., Graham, S. (Eds.), Tectonics, Sedimentary Basins and Provenance: A Celebration of William R. Dickinson's Career. Geological Society of America Special Paper 540, pp. 119–132. https://doi.org/10.1130/2018.2540(06.

Critelli, S., Criniti, S., Ingersoll, R.V., Cavazza, W., 2023. Temporal and Spatial significance of volcanic particles in sand (stone): implications for provenance and paleotectonics. In: Di Capua, A., De Rosa, R., Kereszturi, G., Le Pera, E., Rosi, M., Watt, S.F.L. (Eds.), Volcanic Processes in the Sedimentary Record: when Volcanoes Meet the Environment, vol. 520. Geological Society of London Special Publication, pp. 311–325. https://doi.org/10.1144/SP520-2022-99.

Dalrymple, R.W., Baker, E.K., Harris, P.T., Hughes, M.G., 2003. Sedimentology and stratigraphy of a tide-dominated, foreland-basin delta (Fly River, Papua New Guinea). In: Posamentier, H.W., Sidi, F.H., Darman, H., Nummedal, D., Imbert, P. (Eds.), Tropical Deltas of Southeast Asia – Sedimentology, Stratigraphy, and Petroleum Geology, vol. 76. SEPM Spec. Publ., pp. 147–173

De Ros, L.F., 1998. Heterogeneous generation and evolution of diagenetic quartzarenites in the siluro-devonian furnas Formation of the paraná basin, southern Brazil. Sediment. Geol. 116, 99, 28.

Dickson, J.A.D., 1966. Carbonate identification and genesis as revealed by staining. J. Sediment. Res. 36 (4), 491–505.

Droste, H.J., 1997. Stratigraphy of the lower palaeozoic Supergroup of Oman. GeoArabia 2, 419–471.

Ehrenberg, S.N., 1989. Assessing the relative importance of compaction processes and cementation to reduction of porosity in sandstones: Discussion; Compaction and porosity evolution of Pliocene sandstones, Ventura Basin, California: Discussion. American Association of Petroleum Geologists Bulletin 73, 1274–1276.

Ehrenberg, S.N., 1993. Preservation of anomalously high porosity in deeply buried sandstones by grain-coating chlorite: examples from the Norwegian continental shelf. AAPG (Am. Assoc. Pet. Geol.) Bull. 77 (7), 1260–1286.

Ehrenberg, S.N., Nadeau, P.H., 1989. Formation of diagenetic illite in sandstones of the Garn Formation, Haltenbanken area, mid-Norwegian continental shelf. Clay Miner. 24 (2), 233–253.

El-Ghali, M.A.K., Al-Hinai, N., Mandhari, K., Khan, J., 2019. Diagenesis and reservoir quality of glacio-lacustrine sandstones: an example from the upper carboniferous-lower permian Al khlata Formation in wadi daiqa, northern Oman. In: Boughdiri, M., Bádenas, B., Selden, P., Jaillard, E., Bengtson, P., Granier, B. (Eds.), Paleobiodiversity and Tectono-Sedimentary Records in the Mediterranean Tethys and Related Eastern Areas. CAJG 2018. Advances in Science, Technology & Innovation (IEREK Interdisciplinary Series for Sustainable Development). Springer, Cham, pp. 151–153.

El-Ghali, M.A.K., Mansurbeg, H., Morad, S., Al-Aasm, I.S., Ramseyer, K., 2006a. Distributions of diagenetic alterations in glaciogenic sandstones within depositional facies and sequence stratigraphic framework: evidence from Upper Ordovician of the Murzuq Basin, SW Libya. Sediment. Geol. 190, 323–351.

El-Ghali, Mohamed, A.K., Tajori, Karima G., Mansurbeg, Howri, 2006b. The influence of transgression and regression on the spatial and temporal distribution of diagenetic kaolin in the Upper Ordovician glaciogenic sandstones within a sequence stratigraphic framework, Murzuq Basin, SW Libya. J. Geochem. Explor. 89 (1–3), 87–91, 2006.

El-Ghali, M.A.K., Mansurbeg, H., Morad, S., Al-Aasm, I., Ajdanlisky, G., 2006c. Distribution of diagenetic alterations in fluvial and paralic deposits within sequence stratigraphic framework: evidence from the Petrohan Terrigenous Group and the Svidol Formation, Lower Triassic, NW Bulgaria. Sediment. Geol. 190, 299–321.

El-Ghali, M.A.K., Morad, S., Mansurbeg, H., Caja, M.A., Sirat, M., Ogle, N., 2009. Diagenetic alterations related to marine transgression and regression in fluvial and shallow marine sandstones of the Triassic Buntsandstein and Keuper sequence, the Paris Basin. France. Mar. Petrol. Geol. 26, 289–309.

El-Ghali, M.A.K., El Khoriby, E., Mansurbeg, H., Morad, S., Ogle, N., 2013. Distribution of carbonate cements within depositional facies and sequence stratigraphic framework of shoreface and deltaic arenites, Lower Miocene, the Gulf of Suez rift, Egypt. Mar. Petrol. Geol. 45, 267–280.

El-Khatri, F., El-Ghali, M.A.K., Mansurbeg, H., Morad, S., Neil, O., Robert, K., 2015. Diagenetic alterations and reservoir quality evolution of lower cretaceous fluvial sandstones: nubian formation, Sirt Basin, north-central Libya. J. Petrol. Geol. 38, 217–239.
Folk, R.L., 1968. Petrology of Sedimentary Rocks. Hemphill Publishing Co., Austin, p. 182. USA.
Folk, R.L., Ward, W., 1957. Brazos River bar: a study in the significance of grain size parameters. J. Sediment. Petrol. 27, 3–26.
Forbes, G.A., Jansen, H.S.M., Schreurs, J., 2010. Lexicon of Oman, Subsurface Stratigraphy, vol. 5. GeoArabia Special Publication.
Friedman, I., O'Neil, J.R., 1977. Compilation of Stable Isotope Fractionation Factors of Geochemical Interest, vol. 440. US Government Printing Office.
Furlan, S., Clauer, N., Chaudhuri, S., Sommer, F., 1996. K transfer during burial diagenesis in the mahakam delta basin (kalimantan, Indonesia). Clay Clay Miner. 44 (2), 157–169.
Giles, M.R., Stevenson, S., Martin, S., et al., 1992. The reservoir properties and diagenesis of the Brent Group: a regional perspective. In: Morten, A.C., Haszeldine, R.S., Giles, M.R., Brown, S. (Eds.), Geology of the Brent Group, vol. 61, pp. 289–327 (Special Publication).
Gluyas, J.G., Robinson, A.G., Emery, D., Grant, S.M., Oxtoby, N.H., 1993. The link between petroleum emplacement and sandstone cementation. In: Geological Society, London, Petroleum Geology Conference Series, vol. 4. Geological Society of London, pp. 1395–1402. No. 1.
Hartmann, B.H., Juhasz Bodn ar, K., Ramseyer, K., Matter, A., 2000. Polyphased quartz cementation and its sources: a case study from the Upper Palaeozoic Haushi Group sandstones, Sultanate of Oman. In: Worden, R.H., Morad, S. (Eds.), Quartz Cementation in Sandstones, vol. 29. Int. Assoc. Sedimentol. Spec. Publ, pp. 253–270.
Hayes, M.J., Boles, J.R., 1992. Volumetric relations between dissolved plagioclase and kaolinite in sandstones: implications for aluminum mass transfer in the San Joaquin Basin, California. In: Houseknecht, D.W., Pittman, E.D. (Eds.), Origin, Diagenesis and Petrophysics of Clay Minerals in Sandstones, vol. 47. SEPM Spec. Publ., pp. 111–123
Houseknecht, D.W., 1988. Intergranular pressure solution in four quartzose sandstones. Journal of Sedimentary Petrology 58, 228–246.
Hughes Clarke, M.W., 1988. Stratigraphy and rock unit nomenclature in the oil-producing area of interior Oman. J. Petrol. Geol. 11, 5–60.
Humphreys, B., Kemp, S.J., Lott, G.K., Bermanto, Dharmayanti, D.A., Samsori, I., 1994. Origin of grain-coating chlorite by smectite transformation: an example from Miocene sandstones, North Sumatra back-arck basin, Indonesia. Clay Miner. 29, 681–692.
Jahren, J.S., Aagaard, P., 1989. Compositional variations in diagenetic chlorites and illites and relationships with formation-water chemistry. Clay Miner. 24, 157–170.
Keller, W.D., 1970. Environmental aspects of clay minerals. In: SEPM Journal of Sedimentary Research, vol. 40, 1970.
Land, L.S., Mack, L.E., Milliken, K.L., Lynch, F.L., 1997. Burial diagenesis of argillaceous sediment, South Texas Gulf of Mexico sedimentary basin: a reexamination. Geol. Soc. Am. Bull. 109, 2–15.
Lanson, B., Beaufort, D., Berger, G., Baradat, J., Lacharpagne, J.C., 1996. Illitization of diagenetic kaolinite-to-dickite conversion series; late-stage diagenesis of the Lower Permian Rotliegend Sandstone reservoir, offshore of The Netherlands. J. Sediment. Res. 66 (3), 501–518.
Macaulay, C.I., Haszeldine, R.S., Fallick, A.E., 1993. Distribution, chemistry, isotopic composition and origin of diagenetic carbonates; Magnus Sandstone, North Sea. J. Sediment. Res. 63 (1), 33–43.
Mansurbeg, H., Morad, S., Salem, A., Marfil, R., El-Ghali, M.A.K., Nystuen, J.P., Caja, M. A., Amorosi, A., Garcia, G., Iglesia, A.L., 2008. Diagenesis and reservoir quality evolution of palaeocene deep-water, marine sandstones, the Shetland-Faroes Basin, British continental shelf. Mar. Petrol. Geol. 25, 514–543.
Mansurbeg, H., Morad, S., Plink-Björklund, P., El-Ghali, M.A.K., Caja, M.A., Marfil, R., 2013. Diagenetic Alterations Related to Falling Stage and Lowstand Systems Tracts of Shelf, Slope and Basin Floor Sandstones (Eocene Central Basin, Spitsbergen). Linking diagenesis to sequence stratigraphy, pp. 353–378.
Matlack, K.S., Hous, D.W., 1989. Emplacement of clay into sand by infiltration. SEPM Journal of Sedimentary Research 59.
McBride, M.B., 1989. Reactions controlling heavy metal solubility in soils. In: Advances in Soil Science. Springer, New York, NY, pp. 1–56.
Meisler, H., Leahy, P.P., Knobel, L.L., 1984. Effect of eustatic sea-level changes on saltwater–freshwater in the northern Atlantic coastal plain. US Geological Survey Water-Supply Paper 2255, 28.
Millson, J.A., Quin, J.G., Idiz, E., Turner, P., Al-Harthy, A., 2008. The Khazzan gas accumulation, a giant combination trap in the Cambrian Barik Sandstone Member, Sultanate of Oman: implications for Cambrian petroleum systems and reservoirs. AAPG (Am. Assoc. Pet. Geol.) Bull. 92, 885–917.
Molyneux, S., Osterloff, P., Penney, R., Spaak, P., 2006. Biostratigraphy of the Lower Palaeozoic Haima Supergroup, Oman; its application in sequence stratigraphy nad hydrocarbon exploration. GeoArabia 11, 17–46.
Morad, S., Al-Ramadan, K., Ketzer, J.M., De Ros, L.F., 2010. The impact of diagenesis on the heterogeneity of sandstone reservoirs: a review of the role of depositional facies and sequence stratigraphy. AAPG (Am. Assoc. Pet. Geol.) Bull. 94, 1267–1309.
Morad, S., Ketzer, J.M., De Ros, L.F., 2000. Spatial and temporal distribution of diagenetic alterations in siliciclastic rocks: implications for mass transfer in sedimentary basins. Sedimentology 47, 95–120.
Morad, S., Al-Ramadan, K., Ketzer, J.M., De Ros, L.F., 2010. The impact of diagenesis on the heterogeneity of sandstone reservoirs: a review of the role of depositional facies and sequence stratigraphy. AAPG Bull. 94 (8), 1267–1309.
Moraes, M.A.S., Surdam, R.C., 1993. Diagenetic Heterogeneity and Reservoir Quality: Fluvial, Deltaic, and Turbiditic Sandstone Reservoirs, Potiguar and Reconcavo Rift Basins, Brazil, vol. 77. American Association of Petroleum Geologists Bulletin.
Moraes, M.A.S., De Ros, L.F., 1990. Infiltrated clays in fluvial Jurassic sandstones of Reconcavo Basin, northeastern Brazil. J. Sediment. Petrol. 60, 809–819.
Moraes, M.A.S., De Ros, L.F., 1992. Depositional, infiltrated and authigenic clays in fluvial sandstones of the Jurassic Sergi Formation, Reconcavo Basin, north- eastern Brazil. In: Houseknecht, D.W., Pittman, E.W. (Eds.), Origin, Diagenesis and Petrophysics of Clay Minerals in Sandstones, vol. 47. SEPM Special Publication, pp. 197–208.
Odin, G.S., 1990. Clay mineral formation at the continent-ocean boundary: the verdine facies. Clay Miner. 25 (4), 477–483.
Perez, R.J., Boles, J.R., 2005. An empirically derived kinetic model for albitization of detrital plagioclase. Am. J. Sci. 305 (4), 312–343.
Ramseyer, K., AmthorJ, E., SpotlC, TerkenJ, J.M., MatterA, Vroon ten HoveM, Borgomano, J.R.F., 2004. Impact of basin evolution, depositional environment, pore water evolution and diagenesis on reservoir quality of Lower Paleozoic Haima Supergroup sandstones. Sultanate of Oman: GeoArabia 9, 107–138.
Remy, R.R., 1994. Porosity reduction and major controls on diagenesis of Cretaceous-Paleocene volcaniclastic and arkosic sandstone, Middle Park Basin, Colorado. J. Sediment. Res. 64 (4a), 797–806.
Ryu, I.C., Niem, A.R., 1999. Sandstone diagenesis, reservoir potential, and sequence stratigraphy of the Eocene Tyee Basin, Oregon. J. Sediment. Res. 69 (2), 384–393.
Saïag, J., Brigaud, B., Portier, É., Desaubliaux, G., Bucherie, A., Miska, S., Pagel, M., 2016. Sedimentological control on the diagenesis and reservoir quality of tidal sandstones of the upper cape hay formation (permian, bonaparte basin, Australia). Mar. Petrol. Geol. 77, 597–624.
Shelukhina, O.I., 2021. Depositional Facies, Sequence Straigraphy, and Diagenetic Alterations of a Hybrid-Energy Delta System: an Outcrop Case Study of the Siliciclastic Upper Cambrian-Lower Ordovician Barik Formation, Central Oman. Sultan Qaboos University, Unpublished PhD thesis, p. 288.
Shelukhina, O.I., El-Ghali, M.A.K., Abbasi, I.A., Hersi, O.S., Farfour, M., Ali, A., Al-Awah, H., Siddiqui, N.A., 2021a. Origin and control of grain-coating clays on the development of quartz overgrowths: example from the lower Paleozoic Barik Formation sandstones, Huqf Region, Oman. Arabian J. Geosci. 14, 1–20.
Shelukhina, O., El-Ghali, M.A.K., Abbasi, I.A., Khan, J.A., Khalifa, M.K., Rajendran, S., Al-Sayigh, A., 2021b. Facies architecture and depositional model for a fine-grained hybrid-energy delta: an example from the Upper Cambrian to Lower Ordovician Barik Formation, Central Oman. Geol. J. 56, 4254–42791.
Siddiqui, Numair A., Mathew, Manoj J., Ramkumar, M., Sautter, Benjamin, Usman, Muhammad, Abdul Hadi Abdul Rahman, Mohamed, A., El-Ghali, K., Menier, David, Zhang, Shiqi, Sum, Chow Weng, 2020. Sedimentological characterization, petrophysical properties and reservoir quality assessment of the onshore Sandakan Formation, Borneo. J. Petrol. Sci. Eng. 186, 106771.
Surdam, R.C., Boese, S.W., Crossey, L.J., 1984. The Chemistry of Secondary Porosity: Part 2. Aspects of Porosity Modification.
Surdam et al., 1989 Surdam, R.C., Dunn, T.L., Heasler, H.P., MacGowan, D.B., 1989. Porosity evolution in sandstone/shale systems. In: Hutcheon, I.E. (Ed.), Short Course on Burial Diagenesis, 133. Mineralogical Association of Canada, Montreal, p. 61.
Tanabe, S., Ta, T.K.O., Nguyen, V.L., Tateishi, M., Kobayashi, I., Saito, Y., 2003. Delta evolution model inferred from the Mekong Delta, southern Vietnam. In: Posamentier, H.W., Sidi, F.H., Darman, H., Nummedal, D., Imbert, P. (Eds.), Tropical Deltas of Southeast Asia – Sedimentology, Stratigraphy, and Petroleum Geology, vol. 76. SEPM Spec. Publ., pp. 175–188
Usman, M., Siddiqui, N.A., Mathew, M., Zhang, S., El-Ghali, M.A., Ramkumar, M., Jameel, M., Zhang, Y., 2020. Linking the influence of diagenetic properties and clay texture on reservoir quality in sandstones from NW Borneo. Mar. Petrol. Geol., 104509
Van Keer, I., Muchez, P., Viaene, W., 1998. Clay mineralogical variations and evolutions in sandstone sequences near a coal seam and shales in the Westphalian of the Campine Basin (NE Belgium). Clay Miner. 33 (1), 159–169.
Veizer, J., Ala, D., Azmy, K., Bruckschen, P., Buhl, D., Bruhn, F., Carden, G.A.F., Diener, A., Ebneth, S., Godderis, Y., Jasper, T., Korte, C., Pawellek, F., Podlaha, O.G., Strauss, H., 1999. $^{87}Sr/^{86}Sr$, ^{13}C and ^{18}O evolution of Phanerozoic seawater. Chem. Geol. 161, 59–88.
Wentworth, C.K., 1922. A scale of grade and class terms for classtic sediments. J. Geol. 30 (5), 377–392.
Wilson, M.D., Pittman, E.D., 1977. Authigenic clays in sandstones: recognition and influence on reservoir properties and paleoenvironmental analysis. J. Sediment. Petrol. 47, 3–31.
Wopfner, H., Markwort, S., Semkiwa, P.M., 1991. Early diagenetic laumontite in the lower triassic manda beds of the ruhuhu basin, southern Tanzania. J. Sediment. Res. 61 (1), 65–72.
Worden, R.H., Morad, S., 2000. Quartz Cementation in Oil Field Sandstones: a Review of the Key Controversies, vol. 29. Special Publication-International Association of Sedimentologists, pp. 1–20.
Worden, R.H., Morad, S., 2003. Clay minerals in sandstones: controls on formation, distribution and evolution. In: Worden, R.H., Morad, S. (Eds.), Clay Mineral Cements in Sandstones, vol. 34. Special Publication of the International Association of Sedimentologists, Blackwell, Oxford, pp. 3–41.
Worden, R.H., Griffiths, J., Wooldridge, L.J., Utley, J.E.P., Lawan, A.Y., Muhammed, D. D., Armitage, P.J., 2020. Chlorite in sandstones. Earth Sci. Rev. 204, 103105.
Wright, L.D., 1985. River deltas. In: Davis Jr., R.A. (Ed.), Coastal Sedimentary Environments, 2nd revised expanded edition. Springer-Verlag, Berlin, pp. 1–76.